NATIONAL UNIVERSITY OF SCIENCE AND TECHNOLOGY
POLITEHNICA BUCHAREST
Doctoral School of Aerospace Engineering

DOCTORAL THESIS ABSTRACT

CONTRIBUTIONS TO AERODYNAMIC OPTIMIZATION OF A STRUT-BRACED-WING COMMERCIAL AIRLINER CONFIGURATION

Author: Eng. Mihai-Vlăduț HOTHAZIE
PhD supervisor: Prof. Dr. Eng. Daniel-Eugeniu CRUNȚEANU

DOCTORAL COMMISSION

Chairman	Prof. Dr. Eng. Teodor-Lucian GRIGORIE	from	UNSTPB
PhD. supervisor	Prof. Dr. Eng. Daniel-Eugeniu CRUNȚEANU	from	UNSTPB
Reviewer		from	
Reviewer		from	
Reviewer		from	

BUCHAREST 2025

Acknowledgements

The completion of this doctoral thesis would not have been possible without the support and invaluable guidance of remarkable individuals, whose deep knowledge and constant dedication formed a fundamental pillar in my development as a researcher. Their encouragement and trust inspired me and nurtured my passion for scientific research.

To Prof. PhD. Eng. Daniel-Eugeniu Crunțeanu, I extend my sincere gratitude and profound appreciation for the trust placed in me, scientific guidance, patience, and exceptional professionalism demonstrated throughout the doctoral process. I am especially grateful for his constant availability for meetings, providing unwavering support that significantly enhanced the quality of the results obtained. The additional hours dedicated to the detailed analysis of results reflect a complete commitment to the scientific rigor and excellence of this work.

To CSI PhD. Eng. Mihai-Victor Pricop, I wish to express my deep appreciation and respect for his constant and prompt support, unconditional assistance, and rigorous guidance throughout my doctoral research. I value particularly the insightful advice and expertise provided, which were essential for advancing the results obtained. Moreover, I acknowledge his significant contribution not only to achieving the objectives of this thesis but also to my ongoing professional development, serving as a continuous source of motivation and inspiration.

To Prof. PhD. Eng. Laurențiu Moraru and **Conf. PhD. Eng. Constantin Levențiu,** With deep respect and gratitude, I sincerely thank the advisory committee for their continuous support, constructive suggestions, and valuable advice throughout the preparation of this doctoral thesis. Their contribution was essential in the development of this scientific work.

To PhD. Eng. Ionuț Bunescu, I express my appreciation for his constant support during the entire development of this thesis, particularly in improving ideas related to post-processing, analysis, and interpretation. His professionalism, dedication, and efficiency in scientific research have been a genuine source of inspiration and motivation in my research journey.

To the National Institute for Aerospace Research "Elie Carafoli" - INCAS Bucharest, I extend my sincere thanks to the General Director for the support provided and for facilitating access to the infrastructure necessary to perform the numerical simulations essential for this thesis. I am also grateful to the colleagues who contributed, directly or indirectly, to the successful completion of the presented studies. Additionally, I sincerely thank the institute for the financial support that enabled the dissemination of research results through technical and scientific events, as well as publications in specialized journals.

Finally, I wish to express my heartfelt gratitude to my family and fiancée for their unconditional moral support, patience, profound understanding, and constant encouragement throughout the doctoral process. Their presence and support have been an essential source of strength and motivation during challenging times.

1 INTRODUCTION

The continuous growth of global air traffic is driven by demographic factors and the pivotal role of the aviation sector in facilitating globalization. In this context, regulatory bodies and international programs establish stringent targets for emissions reduction, energy efficiency improvement, and optimization of operational infrastructure, as reflected in initiatives such as NASA N+3 and Flightpath 2050. These programs promote the development of unconventional aircraft configurations with the potential to induce disruptive changes in commercial aircraft design.

One strategy that has recently gained attention is the reduction of induced drag through increased wing aspect ratio, an approach progressively implemented in modern aircraft projects (e.g., Boeing 787, Airbus A350, Boeing 777X). However, structural and operational constraints limit the extension of this solution, motivating intensified research efforts into alternative configurations. Among these, the Strut-Braced Wing (SBW) configuration, originally investigated in the 1950s and subsequently revisited under the SUGAR ("Subsonic Ultra-Green Aircraft Research") program, represents a viable option due to its aerodynamic superiority. Examples such as the Hurel-Dubois HD-31 have demonstrated the feasibility of very high-aspect-ratio wings supported by struts. Currently, major programs, including NASA SUGAR and the X-66 Program, continue to evaluate this configuration, while methodologies developed at Virginia Tech MAD ("Multidisciplinary Analysis and Design") enable the integration of aero-structural effects.

Nevertheless, in the transonic regime, the complexity of aerodynamic phenomena, particularly the formation and interaction of shock waves at the wing-strut junction, leads to a significant increase in drag. Consequently, aerodynamic optimization aimed at minimizing these effects becomes essential, and the development of efficient and robust optimization methodologies constitutes an actively researched area. In this context, the PADRI ("Platform for Aircraft Drag Reduction Innovation") program played a pivotal role by publicly introducing, for the first time, a generic strut-braced wing geometry designed for the collaborative numerical validation of aerodynamic optimization methodologies applied in the transonic regime.

1.1 GENERAL FOUNDATION OF THE STUDY

Globalization has led to a significant increase in air transport, accompanied by complex challenges such as environmental pollution, airspace congestion, and security concerns. Technological advancements and the expansion of computational capabilities have enabled the investigation of unconventional aircraft concepts, among which the strut braced wing configuration has emerged as a promising solution for the short and medium-term. Feasibility and potential studies of this configuration have been conducted by research institutes such as NASA, in collaboration with industrial partners including Boeing and Airbus.

The present research, entitled "Contributions to aerodynamic optimization of a strut-braced-wing commercial airliner configuration" extends existing studies on the evaluation and optimization of the aerodynamic characteristics of strut braced wing configurations. Within the optimization process, five major stages are identified, each of which undergoes detailed analysis and refinement to enhance the overall efficiency of the evaluation and optimization workflow. This undertaking involves a comprehensive examination of geometric parameterization methods, mesh generation techniques, aerodynamic solution methods,

objective function evaluation strategies, and optimization algorithms. The primary goal is to identify the optimal methodology for each stage, thereby reducing the computational effort required to assess the behavior of the objective functions involved in the optimization process.

1.2 OBJECTIVES

The motivation for this work stems from the intensified international efforts in optimizing both conventional and unconventional aircraft configurations, in response to the stringent regulations imposed by aeronautical authorities. Emphasis is placed on developing configurations that can be implemented and operational within a short to medium-term horizon.

In this context, strut braced wing configurations have attracted considerable industrial interest due to their potential to improve aerodynamic performance. The significance of this architecture is reinforced by the active involvement of the aerospace industry, including companies such as Boeing and Airbus, as well as research institutes like NASA and DLR, which invest substantial resources in studying and developing this configuration. Furthermore, the establishment of research programs such as PADRI highlights the scientific and industrial interest in developing efficient aerodynamic optimization methodologies that balance computational cost and runtime, thereby ensuring practical feasibility [21].

However, at the national level, research on transonic aerodynamic optimization remains in its early stages, requiring extensive studies to develop computationally feasible optimization frameworks. Accordingly, this work aims to contribute both nationally and internationally to the development of aerodynamic analysis and optimization methodologies tailored to wing–strut configurations in the transonic regime.

Additionally, the work pursues the following secondary objectives, which support the primary goal:

- Development of a computationally feasible methodology for transonic aerodynamic optimization of unconventional wing–strut aircraft;
- Development and implementation of a differential evolution optimization algorithm, validated using benchmark test functions and evaluated against other commercial algorithms;
- Analysis of the impact of aerodynamic model fidelity, comparing low and high-fidelity simulations on the behavior of the objective function during optimization;
- Automation of the aerodynamic evaluation process through the development of codes for geometry generation, mesh creation, and execution of high-fidelity simulations using both commercial and open-source software;
- Investigation of the feasibility of using neural networks to replace conventional aerodynamic solvers to minimize computational time;
- Conducting a parametric study on the influence of the strut junction geometry on the aerodynamic characteristics of the strut braced wing configuration;
- Optimization of the strut braced wing configuration, developing a computationally efficient optimization methodology;
- Analysis of the impact of nacelle geometry on the aerodynamic characteristics of the optimized configuration, including studies in off-design flight conditions.

1.3 STUDY PHASES AND ORGANIZATION

The study is structured into four main phases:

- Preparatory Phase: A comprehensive analysis of the current state of knowledge in the field is conducted, including a brief historical overview and the current international context. The theoretical foundations of optimization processes are presented, along with their associated stages, and the principles for developing a dedicated optimization code, which will be employed in the subsequent phases of the study.
- Phase on the Influence of Model Fidelity: This phase includes an extensive analysis of the impact of aerodynamic analysis model fidelity on the behavior of the objective function. The feasibility of replacing flow modeling with a neural network trained on a high-fidelity dataset is also investigated.
- Aircraft Configuration Optimization Phase: This phase aims to optimize the wing–strut aircraft configuration using a cascade methodology, which includes: conducting a parametric study on the influence of geometric parameters in the wing–strut junction, analyzing the objective function behavior, optimizing the strut airfoil in the presence of the wing profile based on the accumulated information, and performing a three-dimensional optimization of the junction region within the full aircraft configuration.
- Validation Phase: The aerodynamic characteristics obtained from the optimization process are compared with those of the reference configuration. This includes analyzing off-design behavior and evaluating the influence of the nacelle geometry on aerodynamic performance.

The thesis is organized into four main chapters:

- Chapter 1: Introduction, motivation for the research topic, and definition of the specific research objectives.
- Chapter 2: A detailed analysis of the current state of knowledge in aerodynamic optimization, including historical evolution, the current international status, and essential theoretical foundations.
- Chapter 3: Methodologies applied in the research, development and validation of the optimization codes, validation of automation codes for aerodynamic evaluation, and studies on the influence of model fidelity on optimization performance. This chapter also details the aerodynamic optimization of the wing–strut configuration using a cascade approach, including parametric studies, two and three-dimensional optimizations, and validation of the results through comparisons with experimental data and numerical simulations from the literature. Additionally, the effects of nacelle inclusion on aerodynamic characteristics in both reference and off-design flight regimes are analyzed, providing a comprehensive overview of the optimized configuration’s performance.
- Chapter 4: Conclusions and original contributions of the study, followed by a list of scientific publications and technical presentations derived from the research, as well as a discussion on potential directions for future development.

2 STATE OF THE ART STUDY

This chapter presents both the chronological evolution of studies in the field and the theoretical foundations necessary to understand the investigations conducted in this work. The chapter is structured to facilitate the transition from general and historical concepts to the technical principles underlying the studies presented in the thesis.

The first subsection is dedicated to analyzing the evolution of strut braced wing (SBW) configurations, tracing their initial appearances and early applications in the field. This review of development trends for wing–strut configurations provides the necessary context for understanding the motivation and justification for the studies presented in this thesis.

The second subsection synthesizes recent results and trends from the literature, analyzing major contributions from the last few years. Theoretical, experimental, and numerical approaches currently used in research are discussed, as well as the primary areas of interest for the international scientific community. This subsection aims to present contemporary methodologies, highlighting their advantages and limitations.

The third subsection establishes the theoretical foundation required for aerodynamic optimization processes, detailing the essential stages of such endeavors, the corresponding methods for each stage, and the advantages and limitations associated with various approaches. It is organized into four main sections:

Section 2.3.1 provides a comparative analysis of different geometric parameterization methods available in the literature, applicable to both airfoils and three-dimensional wing configurations. The advantages, limitations, and domains of applicability of each method are discussed, emphasizing the selection criteria relevant to this study.

Section 2.3.2 describes the strategies for generating computational grids used in high-fidelity aerodynamic analysis. The process of geometry discretization, mesh types (structured, unstructured, hybrid), and efficient mesh regeneration methods are detailed with respect to computational cost.

Section 2.3.3 presents the numerical models used in aerodynamic analysis, ranging from low-fidelity models based on simplified theories to high-fidelity models. The assumptions, limitations, and applicability of each model are discussed, with emphasis on the trade-off between computational cost and accuracy of results.

Section 2.3.4 classifies and presents the main optimization methods, distinguishing between deterministic and stochastic approaches. This section also details the theoretical foundations of the differential evolution algorithm implemented in this work using a parameter-free penalty scheme.

Overall, this chapter provides the theoretical framework of the thesis, justifying the selected research directions and presenting the essential concepts underlying optimization processes. These foundations are subsequently applied in the following chapter for the development of numerical studies dedicated to optimizing the strut-braced-wing configuration analyzed in this work.

3 NUMERICAL STUDY

3.1 COMPARATIVE STUDY BETWEEN LOW AND HIGH FIDELITY SIMULATIONS

This study investigates the accuracy and efficiency of different aerodynamic analysis methods employed within an airfoil optimization process, aiming to highlight the advantages and limitations of each approach in the context of selecting the most appropriate method for subsequent studies presented in this thesis. The optimization process was based on an in-house code implementing a differential evolution algorithm with a parameter-free penalty scheme, validated against standard benchmark test functions from the literature, as illustrated in Fig. 3.1.

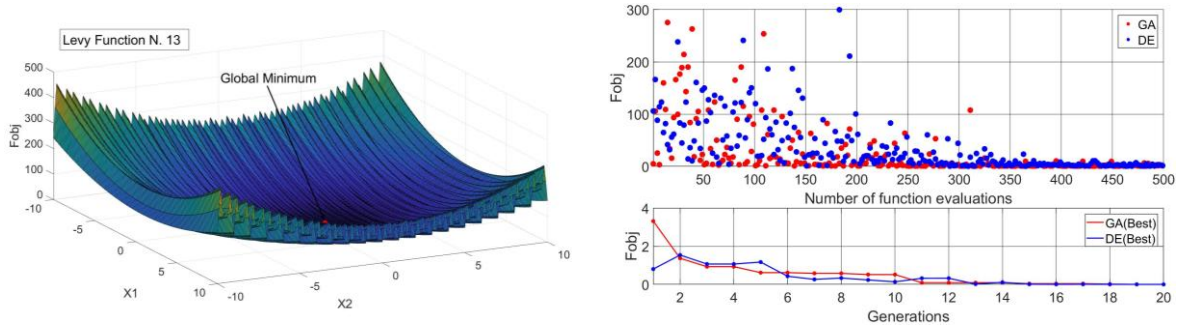

Fig. 3.1. Representation of the Levy Function N.13 test function along with the convergence process histograms for the DE and GA algorithms.

To comprehensively evaluate the robustness and performance of the proposed algorithm, it was compared with a classical genetic algorithm available in the MATLAB toolbox, using identical initial conditions and optimization constraints. Following validation with benchmark test functions from the literature, the algorithm was employed in a comparative study to assess the influence of aerodynamic model fidelity on the airfoil optimization process. The automation of objective function evaluation was implemented for two analysis tools: XFOIL (low-fidelity, short computational time) and ANSYS Fluent (high-fidelity, significantly longer computational time).

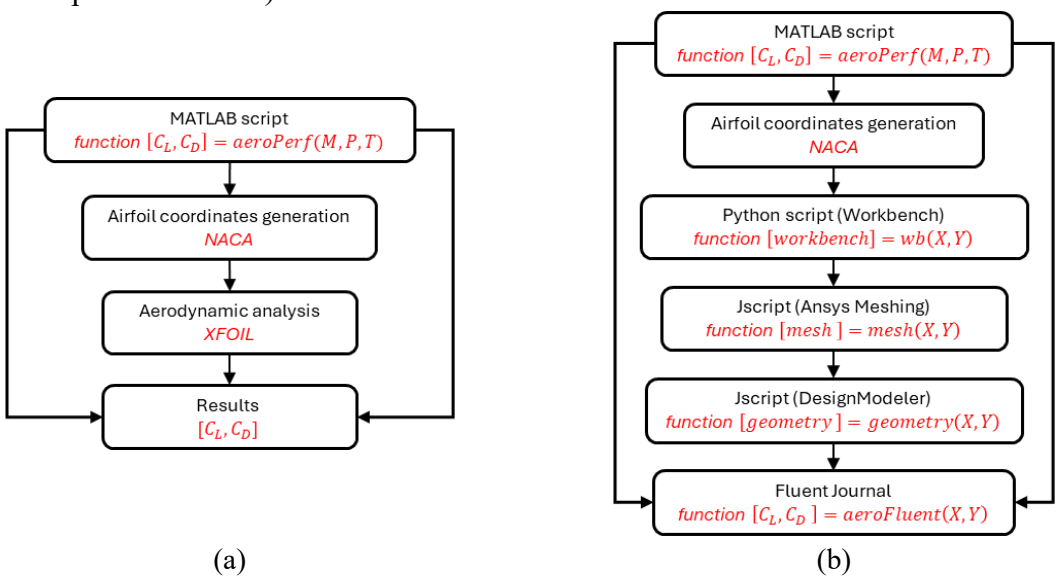

(a) (b)

Fig. 3.2. Logical scheme of the automation process used for the Xfoil (a) and the Fluent (b)

To simplify the process and reduce computational effort, the NACA 4-digit parameterization method was selected. The optimization aimed at maximizing C_L/C_D for a

representative case, assuming steady, incompressible, and fully turbulent flow at $Re = 6\times10^6$, $V = 51$ m/s, $\rho = 1.77$ kg/m³, $\mu = 1.645\times10^{-5}$ kg/(m·s), and an angle of attack $\alpha = 2°$. The computational domain was discretized in ANSYS Meshing with a prismatic boundary layer grid ($y^+ \approx 1$, 40 layers, growth rate 1.1), and CFD simulations were performed in ANSYS Fluent using the RANS equations coupled with the k–ω SST turbulence model.

For robust validation of the optimization algorithm, both for the low-fidelity method (XFOIL) and the high-fidelity method (ANSYS Fluent), a convergence study was conducted with respect to the initial population size. The population sizes considered in the parametric study were 12, 25, 50, and 100 individuals. This was necessary due to the lack of prior information on the objective function behavior, making it important to assess the algorithm's sensitivity to this parameter.

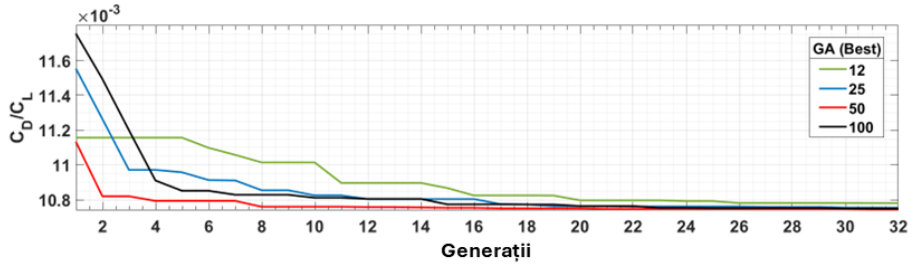

(a)

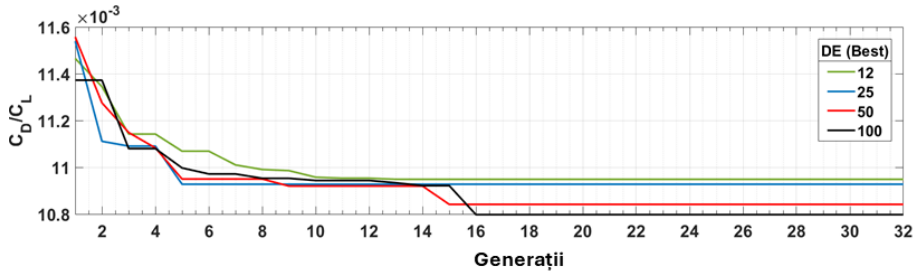

(b)

Fig. 3.3. Convergence process histograms for the DE and GA algorithms, as a function of the initial population size, evaluated with Ansys Fluent

A comparative analysis of the objective function behavior was also conducted using the XFOIL analysis tool. In contrast to the Fluent-based analyses, significant differences were observed both in the objective function values and in its overall behavior. Specifically, the range of C_L/C_D values is nearly twice that obtained with Fluent, and the function exhibits multiple intersection regions among planes corresponding to the parameter P. These observations confirm the multimodal and noisy nature of the objective function when using XFOIL, which explains the convergence difficulties previously noted for both optimization algorithms.

This highlights the importance of employing a high-fidelity analysis tool whenever computational resources allow. Furthermore, the introduction of geometric or aerodynamic constraints can significantly restrict the search space, potentially altering its topology entirely. In such cases, the influence of the chosen analysis tool on the optimization results becomes even more pronounced, underscoring the necessity of high-fidelity flow modeling in the context of optimization studies.

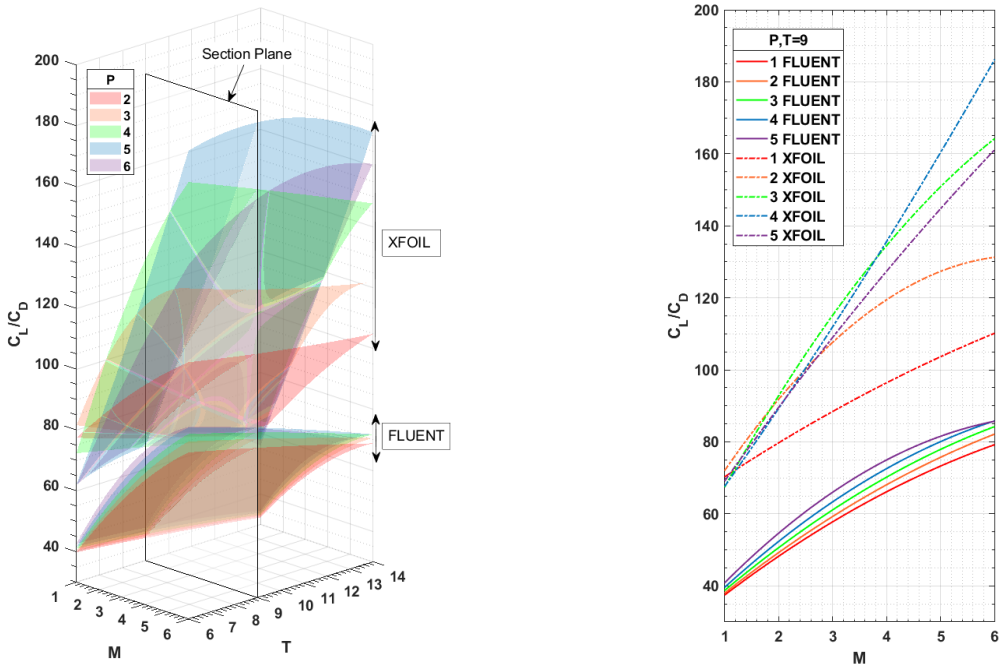

(a) (b)

Fig. 3.4. Representation of the C_L/C_D ratio behavior in plane view (a) and in cross-section (b)

The procedure for automating the aerodynamic evaluation of NACA 4-digit airfoils using ANSYS Fluent was extended by including the angle of attack as an additional parameter, enabling exploration of the design space and assessment of the feasibility of applying artificial intelligence methods. The resulting dataset was used to train a feedforward neural network with six layers: one input layer, four hidden layers, and one output layer. The input layer comprises four neurons corresponding to the parameters M (maximum camber), P (position of maximum camber), T (maximum thickness), and α (angle of attack), the hidden layers each contain ten neurons, and the output layer has two neurons for the aerodynamic coefficients C_L and C_D. This architecture provides an efficient modeling of the nonlinear relationships between the parameters and the coefficients, ensuring a balance between computational cost and generalization capability. The dataset was split into 80% for training and 20% for testing to evaluate the model's performance.

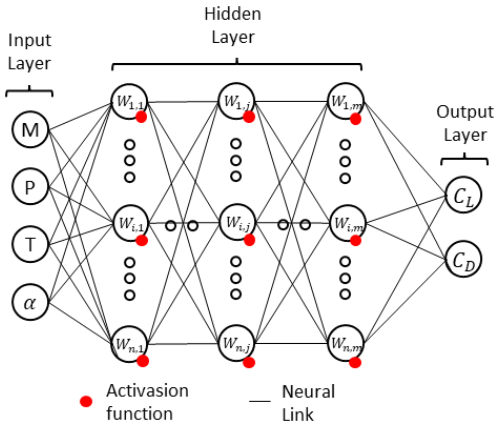

Fig. 3.5. Neural network architecture

Fig. 3.6 presents a comparison between the lift coefficient C_L and drag coefficient C_D values predicted by the neural network and the reference values from the database generated using Fluent simulations.

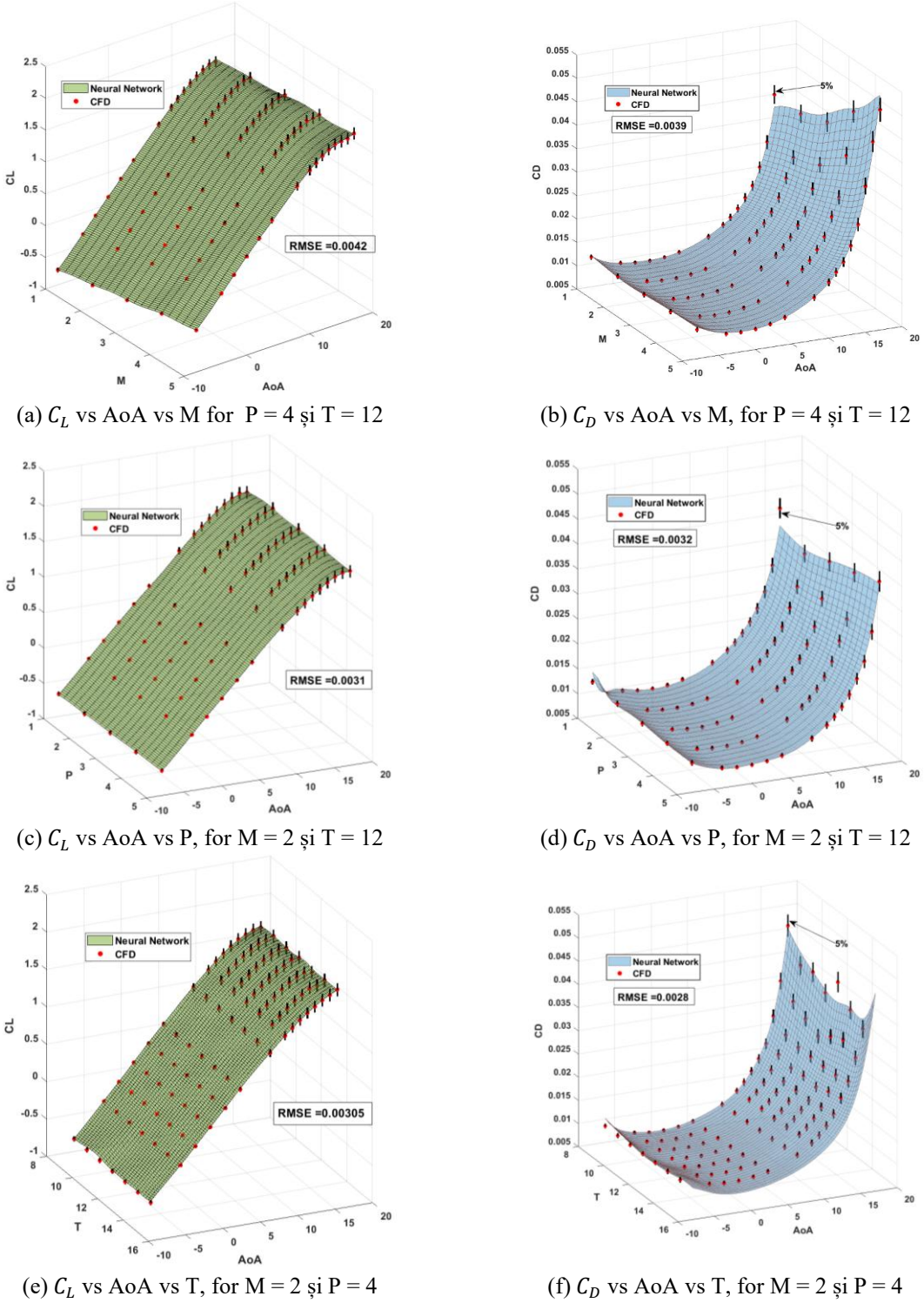

(a) C_L vs AoA vs M for P = 4 și T = 12

(b) C_D vs AoA vs M, for P = 4 și T = 12

(c) C_L vs AoA vs P, for M = 2 și T = 12

(d) C_D vs AoA vs P, for M = 2 și T = 12

(e) C_L vs AoA vs T, for M = 2 și P = 4

(f) C_D vs AoA vs T, for M = 2 și P = 4

Fig. 3.6. Comparative parametric study of aerodynamic characteristics of NACA 4-digit airfoils using Fluent and Neural Network predictions

Although the neural network training time was short (on the order of tens of minutes), generating the corresponding database required a significant computational effort, lasting several days. This highlights that, while the network can accurately predict the aerodynamic characteristics of NACA 4-digit airfoils, database generation is not feasible for conventional optimization tasks. However, in multi-objective or constrained optimizations, where the objective function must be evaluated multiple times, the network proves to be highly efficient. In this context, a Constrained Multi-Objective Genetic Algorithm (gamultiobj) from MATLAB was employed, with an initial population of 50 individuals. The evaluation of a single individual

takes approximately 0.05s, demonstrating the network's efficiency. The results include the Pareto fronts obtained for the different combinations of objective functions.

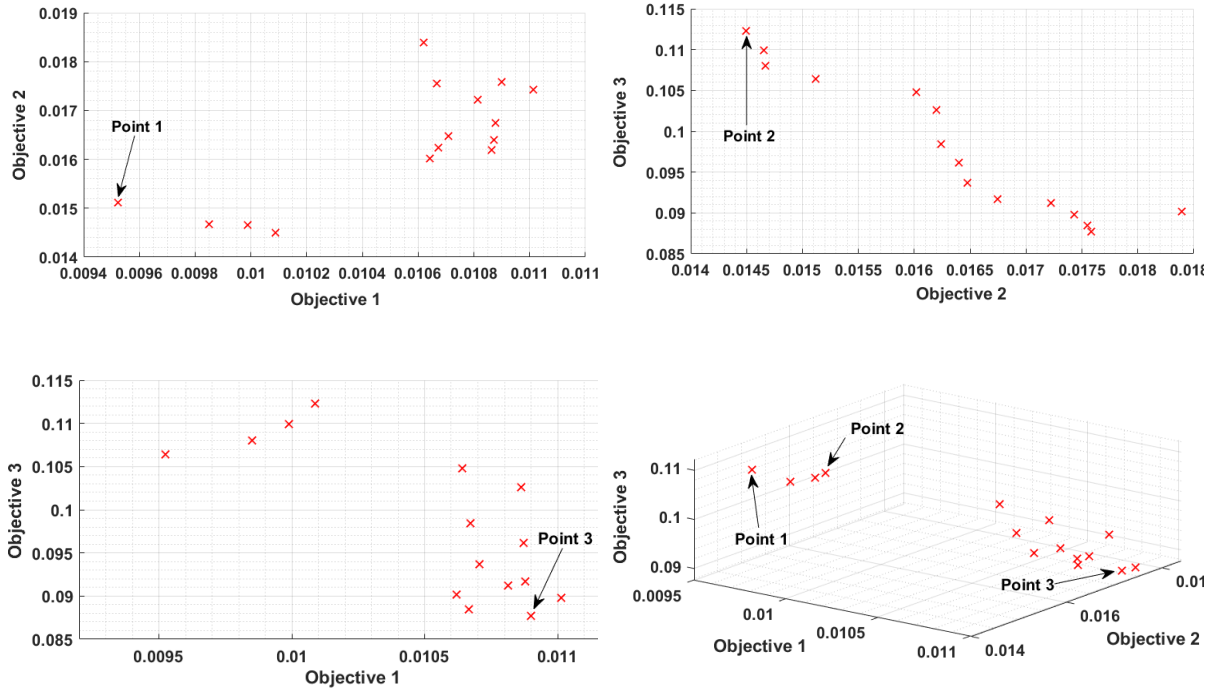

Fig. 3.7. Representation of the Pareto front

Within the multi-objective genetic algorithm, the optimal solutions lie along the Pareto front, each representing a trade-off between the objective functions, which necessitates the analysis of multiple outcomes for optimal selection. The geometric representation of the three selected optimal points highlights the influence of geometric parameters on aerodynamic characteristics. Although the position of maximum camber (P) remains consistent across solutions, significant variations are observed in the maximum camber value (M), emphasizing the impact of this parameter on aerodynamic performance.

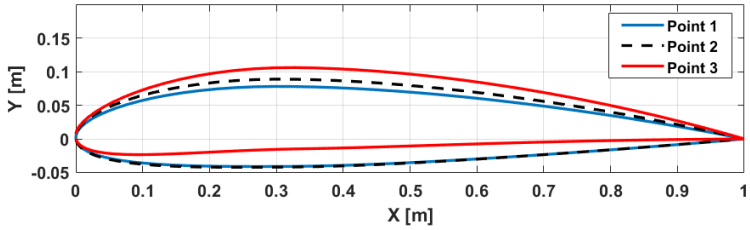

Fig. 3.8. Geometric representation of the three selected optimal points

For additional validation, the optimized airfoils were evaluated using ANSYS Fluent, demonstrating that the neural network accurately predicts aerodynamic characteristics with maximum errors below 3%. Due to the short evaluation time and minimal computational effort, the neural network proves highly efficient for multi-objective optimizations involving multiple constraints and numerous objective function evaluations. Conversely, for simpler optimization problems with few constraints, directly using a high-fidelity solver such as Fluent is more feasible than generating a database and training the neural network.

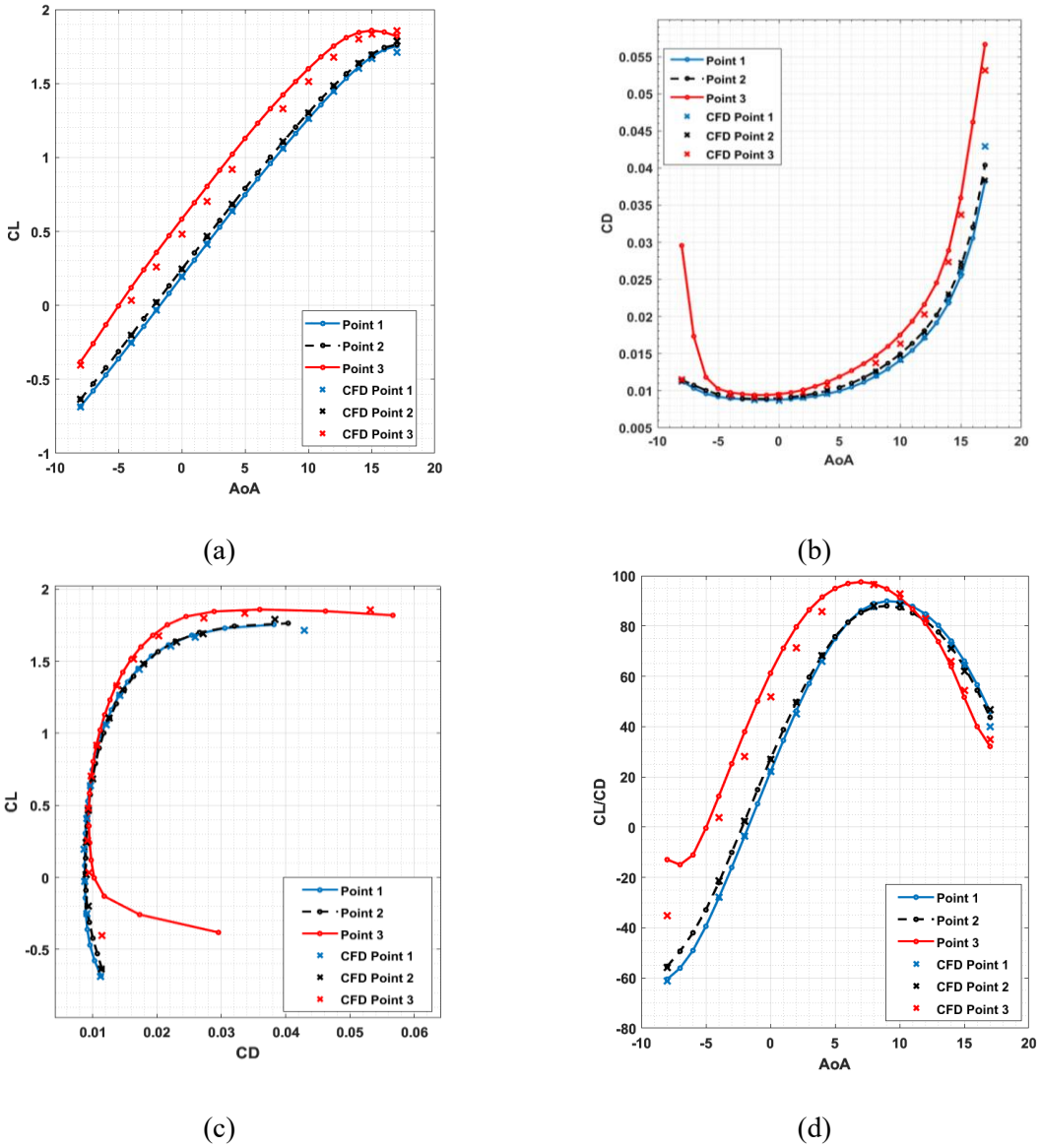

Fig. 3.9. Comparison of the three optimal airfoils obtained: (a) C_L vs α, (b) C_D vs α, (c) C_L vs C_D și (d) C_L/C_D vs α

For the validation of the transonic optimization methodology, the RAE2822 airfoil was selected as a reference case with available experimental and numerical data in the literature. Simulations were conducted at Re = 6.5×10^6, M = 0.729, and α = 2.31°, with the optimization objective being the reduction of drag while maintaining the lift coefficient and airfoil area as constraints. The airfoil geometry was parameterized using the Class-Shape Transformation (CST) method, with three parameters for both the upper and lower surfaces, resulting in six design variables. Due to the size of the design space and the presence of constraints, a stochastic Differential Evolution (DE) algorithm was employed, effective for multimodal and potentially discontinuous objective functions. To minimize computational effort, CFD simulations were performed using ADFlow, a high-fidelity open-source solver developed at the MDO LAB.

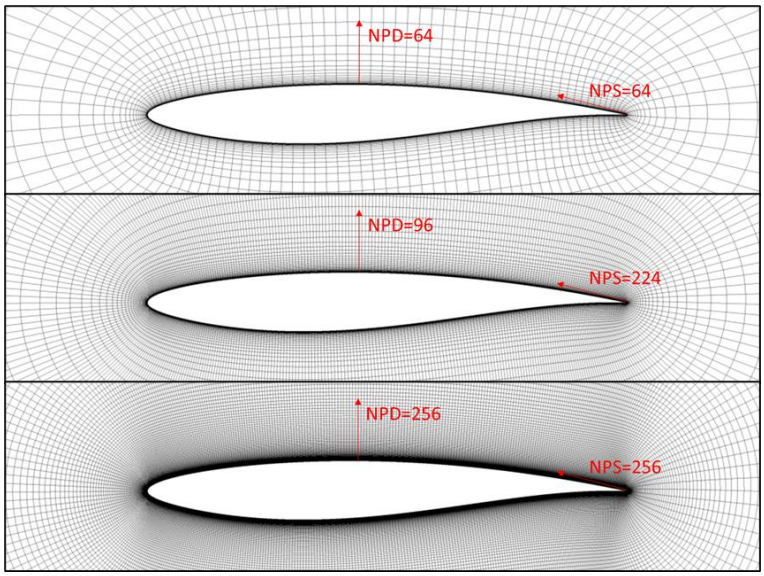

Fig. 3.10. Representation of hyperbolic grids of coarse, medium, and fine types.

To enforce the lift coefficient constraint, a grid convergence study was conducted with respect to NPS (number of points along the surface) and NPD (number of points in the wall-normal direction). Fig. 3.10 illustrates three grids, fine, medium, and coarse, highlighting the differences between them. Fig. 3.11 presents the convergence study, showing that a grid resolution of 224 × 96 points achieves a favorable balance between computational cost and accuracy, providing an optimal compromise for the optimization process.

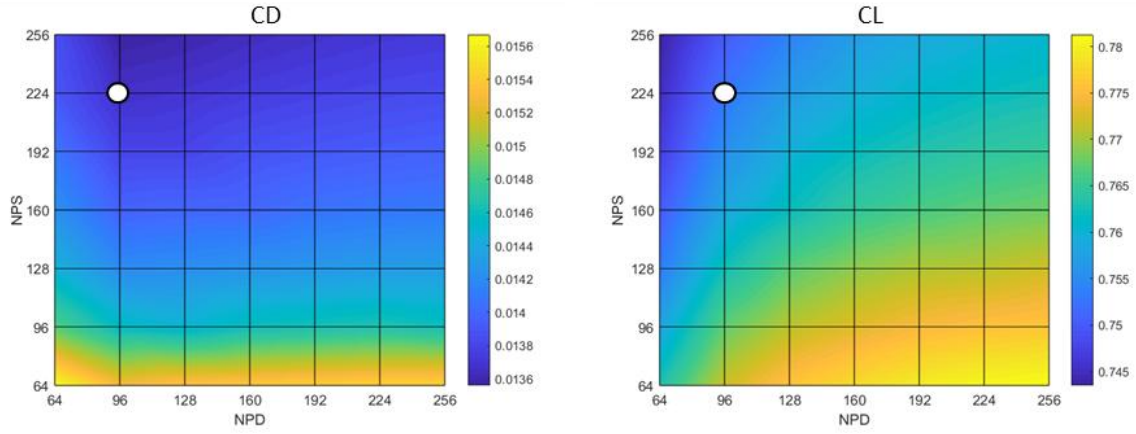

(a) (b)

Fig. 3.11. Convergence plots as a function of grid parameters for aerodynamic performance: drag coefficient (a) and lift coefficient (b)

Table 3.1 presents the results obtained from the numerical simulations, compared with the reference experimental data available in the literature for the RAE2822 airfoil under the specified flight conditions. The comparison focuses on the lift coefficient C_L and the drag coefficient C_D , along with their associated relative errors. The results indicate a relative error of approximately 1% for the lift coefficient and about 7% for the drag coefficient, values that are acceptable in the context of transonic flight conditions, where both grid resolution and the turbulence model can introduce discrepancies.

Tabel 3-1. Validation of the obtained results against reference data

Case	M_∞	Grid size	First cell height	C_D	C_L	$C_D err$[%]	$C_L err$[%]
Numeric	0.729	224x96	5e-05	0.0136	0.752	7%	1.2%
Experimental [60]	0.729	-	-	0.0127	0.743	-	-

For further validation of the obtained numerical solution, the pressure coefficient distribution was analyzed and compared with both experimental reference data and numerical results available in the literature, obtained using the CFD code WIND, developed by the NPARC Alliance. This comparison allowed assessment of the numerical solution's fidelity not only at the global level through aerodynamic coefficients but also locally by predicting the location and intensity of the shock wave. Additionally, results corresponding to multiple turbulence models were presented to illustrate the impact of the turbulence model on the pressure distribution. Specifically, the comparison included results obtained using the algebraic Baldwin–Lomax model, the Spalart–Allmaras one-equation transport model, and the k–ω SST (Shear Stress Transport) two-equation transport model, all implemented in the WIND code.

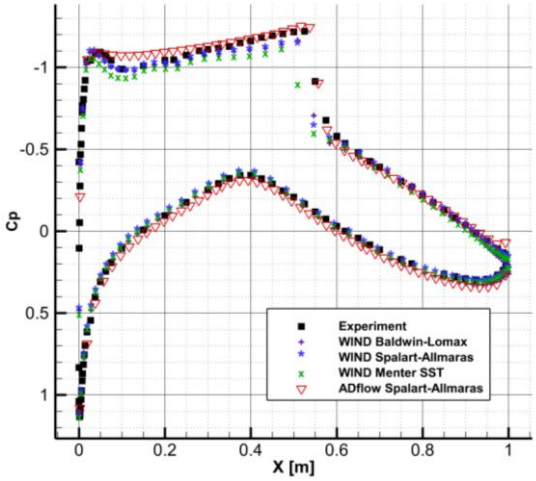

Fig. 3.12. Comparison of the pressure coefficient distribution between experimental and numerical results [60].

Considering the convergence study and the comparison of the pressure coefficient distribution, the optimization problem can be formulated as follows:

$$\begin{aligned} &minimize\ f(x) = C_D \\ &subjected\ to: \quad Area_{opt} \geq Area_{RAE\ 2822} \\ &\qquad\qquad\quad C_{L_{opt}} = 0.75 \end{aligned} \tag{3.1}$$

Fig. 3.13 illustrates the geometry obtained through the constrained optimization process in comparison with the reference RAE2822 airfoil. A reduction in the maximum thickness and a rearward shift toward the trailing edge are observed. Additionally, the maximum camber of the airfoil is reduced, indicating a decrease in the pressure gradient on the upper surface, which suggests a reduction in fluid acceleration and, consequently, a decrease in shock intensity.

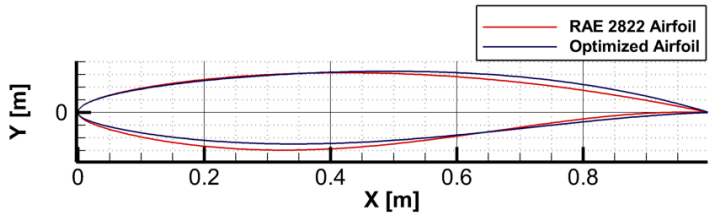

Fig. 3.13. Comparison between the optimized airfoil geometry and RAE2822.

The analysis of the convergence history presented in Fig. 3.14 highlights the emergence of a stable plateau starting from generation 36, indicating that an optimal solution has been reached. The behavior of both the best individual in each generation and the population mean demonstrates clear and consistent convergence, suggesting a continuous search space without multiple local minima. This observation indicates that the objective function exhibits a quasi-unimodal character, dominated by a well-defined global optimum. Consequently, for the transonic regime under study, the optimization of airfoil profiles would benefit from employing a deterministic algorithm based on the conjugate gradient method, which could significantly reduce computational effort and overall calculation time.

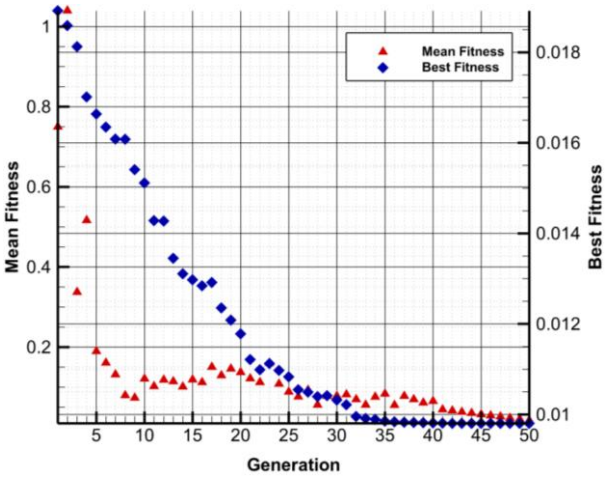

Fig. 3.14. Convergence history of the objective function vs. generations

Table 3.2 presents the aerodynamic characteristics of the optimized airfoil in comparison with the RAE 2822 profile. The results indicate a significant improvement in the drag coefficient, with a reduction of approximately 28%. Additionally, the lift coefficient constraint is satisfied with a margin of error of 0.13%, demonstrating the feasibility of the obtained solution.

Tabel 3-2. Performance of the baseline vs. optimized configuration

Case	M_∞	Grid size	First cell height	C_D	C_L	$C_D err$[%]	$C_L err$[%]
RAE2822	0.729	224x96	5e-05	0.0136	0.752	-	-
Optimized	0.729	224x96	5e-05	0.0098	0.751	-27.94%	-0.13%

Comparing the distributions of the pressure coefficient (C_p) and the skin friction coefficient (C_f) between the RAE2822 airfoil and the optimized airfoil reveals a significant reduction in shock intensity, while maintaining feasibility constraints. Additionally, a favorable recovery of the pressure coefficient downstream of the shock is observed, indicating boundary layer re-energization and fluid acceleration. Analysis of the region below the critical pressure coefficient C_p^* shows a decrease in flow deceleration induced by the shock, while the C_f

distribution exhibits a reduction before the shock and an increase immediately afterward, suggesting that the relocation of the maximum camber toward the trailing edge contributed to fluid acceleration in the optimized region.

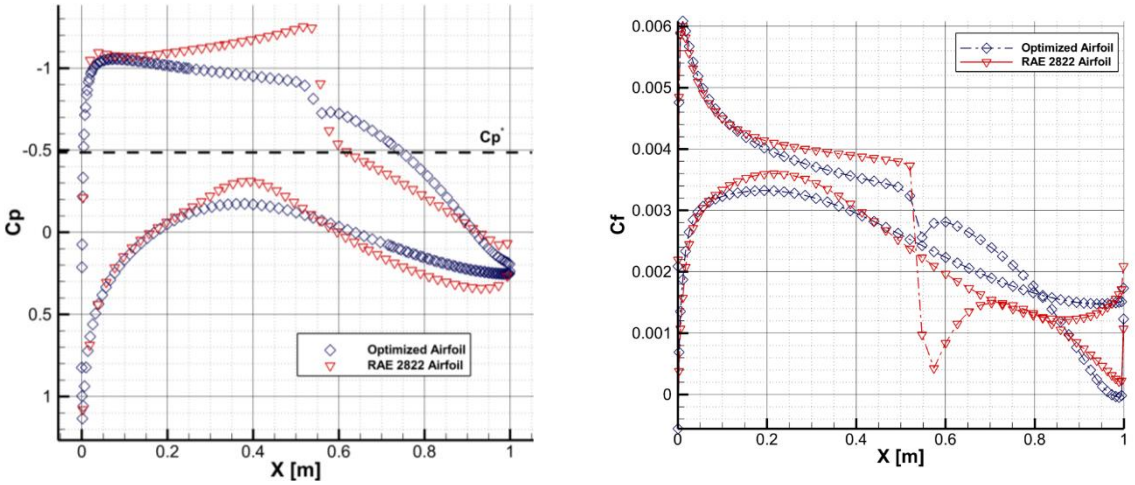

Fig. 3.15. Comparison between the optimized airfoil and RAE2822: (a) pressure coefficient (C_p) distribution and (b) skin friction coefficient (C_f) distribution.

3.2 PADRI CONFIGURATION OPTIMIZATION

Building on the insights gained regarding the feasibility of using both low and high-fidelity aerodynamic solvers, as well as their influence on the objective function behavior under subsonic and transonic flow regimes, the optimization process was extended to a full aircraft configuration with a wing–strut arrangement.

In the initial stage, the results obtained for the PADRI reference configuration were compared with data available in the literature, and a grid convergence study was conducted to validate the numerical solution accuracy. The configuration analyzed includes the wing, strut, and fuselage assembly, based on the geometry provided by the PADRI platform, which aims to support the development and validation of aerodynamic optimization methodologies. The main objective of this study was to identify effective methods for reducing shock-wave interference in the wing–strut junction region and to minimize wave drag associated with this area. Subsequently, a parametric study of the strut geometry was conducted to evaluate its influence on the aerodynamic characteristics of the configuration and on shock-wave interactions under transonic conditions. Based on the findings, a two-stage optimization methodology was developed:

- *Two-dimensional optimization:* This stage focused on optimizing the strut's airfoil in the presence of the wing's airfoil. The objective function was defined using information extracted from the parametric study, taking into account local interactions and pressure distributions.
- *Three-dimensional optimization:* In this stage, the previously optimized strut geometry was refined, considering three-dimensional flow effects in the full configuration to eliminate supersonic regions in the wing–strut junction.

This methodology allows extracting the information necessary for optimizing strut braced wing configurations, using a search space exploration of the strut parametric geometry, followed by a two-dimensional optimization for global refinement of the strut geometry, and finally a three-dimensional refinement to completely remove supersonic regions between the strut and wing.

The first step involved validating the numerical results by comparing them with available literature data for the PADRI reference configuration. The analyzed reference case corresponds to a transonic flight regime, with Mach number M=0.72, altitude H=30000 ft and angle of attack α=1°. The publicly available PADRI configuration for analysis includes the wing, strut, and fuselage. The geometric representation of the analyzed configuration is shown in Fig. 3.16.

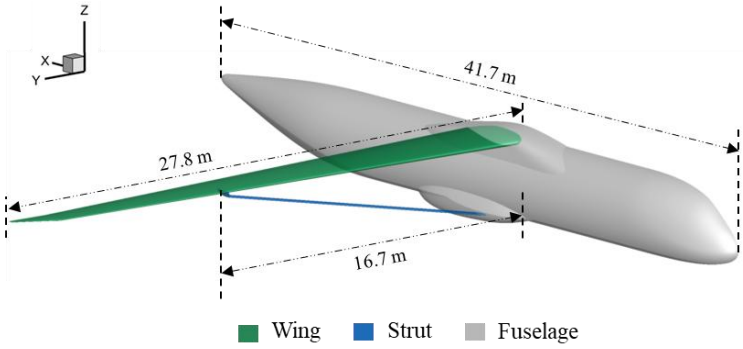

Fig. 3.16. Geometric representation of the PADRI semi-model configuration

For the computational grid generation, an unstructured approach was adopted, justified by the geometric complexity of the configuration. The surface grid generation process was divided into four regions corresponding to the fuselage, wing, strut, and wing–strut junction.

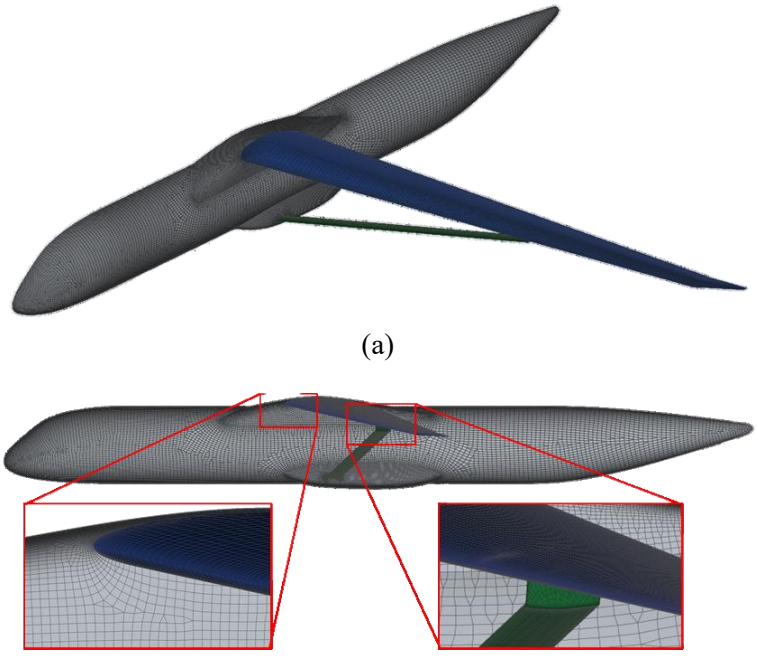

(a)

(b)

Fig. 3.17. Surface grid representation used for volume grid generation: (a) isometric view and (b) side view

For the generation of the volume mesh, the boundary layer region was discretized based on the previously generated surface mesh, using predominantly hexahedral prismatic elements created through an inflation-type algorithm. The volume mesh, along with a representative section of the computational domain, is shown in Fig. 3.18, highlighting the symmetry plane, the boundary layer region, and the interior zone generated via the Hexa-Interior algorithm. This representation allows a visual assessment of the mesh quality and the element distribution relative to the regions of interest.

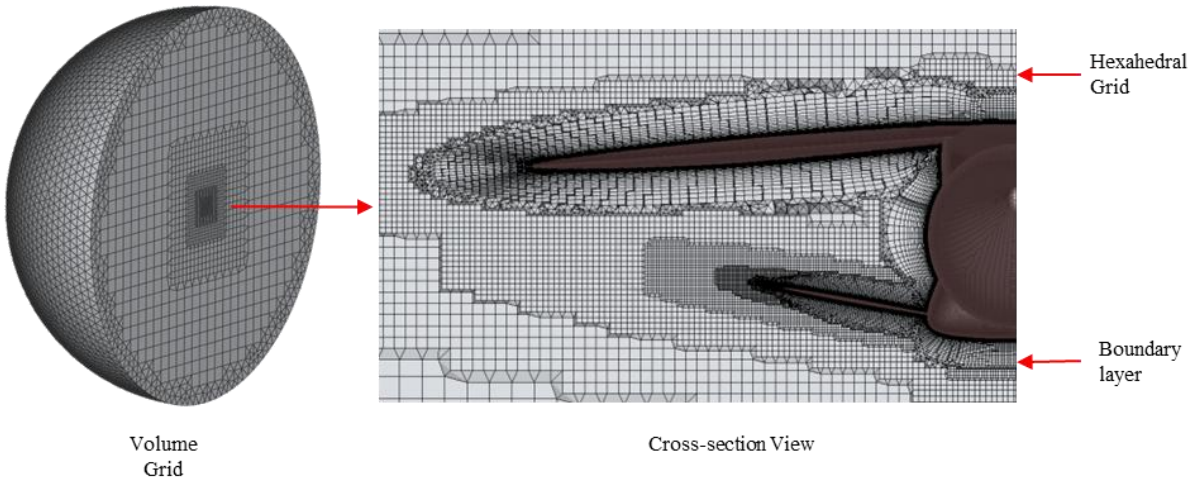

Fig. 3.18. Volume grid and representative computational domain highlighting the symmetry plane, boundary layer region, and interior volume generated using the Hexa-Interior algorithm.

The numerical simulations were carried out using the ANSYS Fluent aerodynamic solver by solving the RANS equations coupled with the k–ω SST turbulence model. Pressure far-field boundary conditions were applied at the domain boundaries. For the grid convergence

study, three levels of refinement were generated: coarse, medium, and fine. This procedure aimed to evaluate the influence of element size on the numerical solution accuracy and to identify a compromise configuration between solution fidelity and computational cost. Following the comparative analysis, the medium grid was selected as the optimal choice, providing a balance between accuracy and computational efficiency. This grid configuration was subsequently adopted for both the parametric study of the strut geometry and the optimization processes. Additionally, the results were compared with those reported in [32], which employed structured multi-block overset grids with a Spalart–Allmaras one-equation turbulence model, solved using ADFlow.

Tabel 3-3. Grid convergency study

Case	M_∞	Grid size [mil]	Δs	C_D [$\times 10^{-4}$]	C_L	C_D *err* [%]	C_L *err* [%]
1	0.72	5.3	8e-05	238	0.368	5.8%	7.8%
2		9.5		227	0.402	0.9%	0.8%
3		13.5		225	0.399	-	-
4 [32]		5.6	-	228.5	0.405	-	-

The analysis indicated that a grid with 9.5 million elements provides an optimal compromise between computational cost and solution accuracy. The error associated with the medium grid, compared to the fine grid, is below 1% for both the drag coefficient C_D and the lift coefficient C_L , as shown in Table 3-3.

Subsequently, a parametric study was conducted to evaluate the influence of the strut geometry on the aerodynamic behavior of the configuration. The analysis considered two main parameters: the length L and the tilt angle θ, which characterize the geometry of the strut–wing junction. These parameters were chosen because they control the size of the channel formed between the wing and the strut, as well as the spanwise flow behavior. The analyzed parameters are illustrated in the figure below, highlighting the design space explored in the parametric study and the geometric modifications that can affect aerodynamic interactions in the wing–strut junction region.

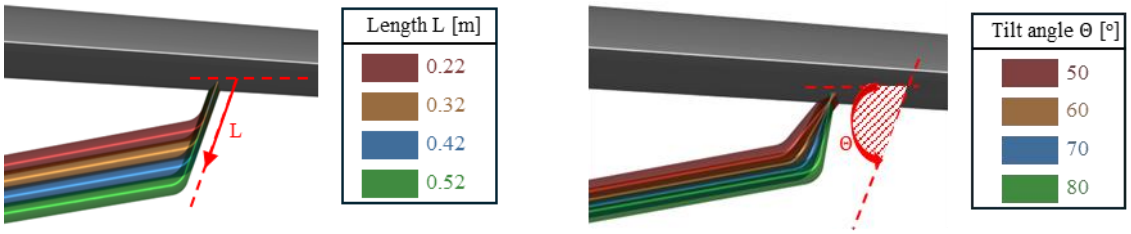

(a) (b)

Fig. 3.19. Parameter representation: (a) strut length L, (b) tilt angle θ

The influence of the geometric parameters was evaluated for four angles of attack, ranging from α=0° to α=3°. Starting from the reference geometry (L=0.32 m, θ=70°), the strut length L was varied between 0.22 m and 0.52 m in increments of 0.1 m, while the tilt angle θ was modified from 50° to 80° in steps of 10°. In total, 28 distinct cases were analyzed.

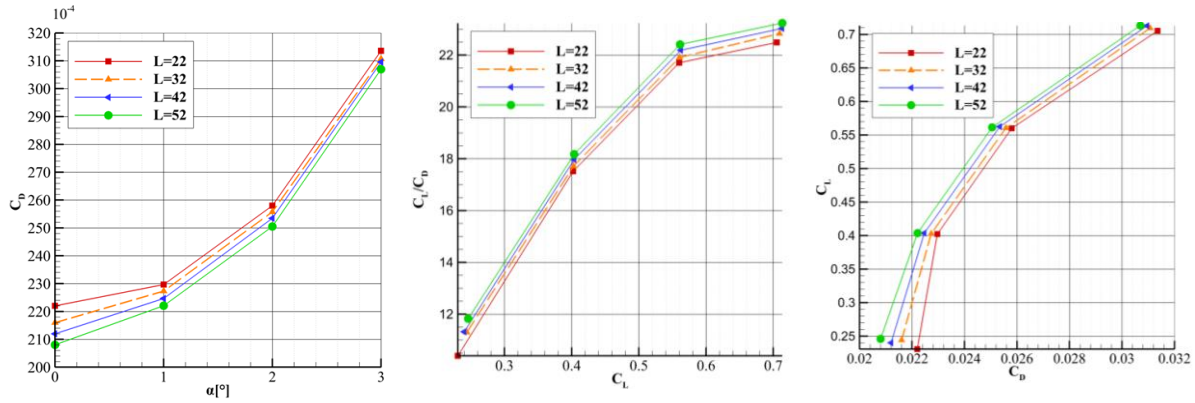

(a) (b) (c)

Fig. 3.20. Variația C_D vs α (a), C_L/C_D vs C_L (b) și C_L vs C_D (c) în funcție de parametrul L

For a deeper understanding of the influence of the parameter L, Fig. 3.21 presents visualizations of the shockwave isosurfaces using the method proposed by Lovely and Haimes, an approach similar to that of reference [32].

$$Ma_n = \frac{Ma \cdot \nabla p}{|\nabla p|} = \frac{\mathrm{V} \cdot \nabla \mathrm{p}}{|\nabla p|} \tag{3.2}$$

Fig. 3.21 illustrates the variation of supersonic regions as a function of the length parameter L, while maintaining an inclination angle of θ=70° at an angle of attack α=1°. For visualization, an isosurface corresponding to M=1.1 was used.

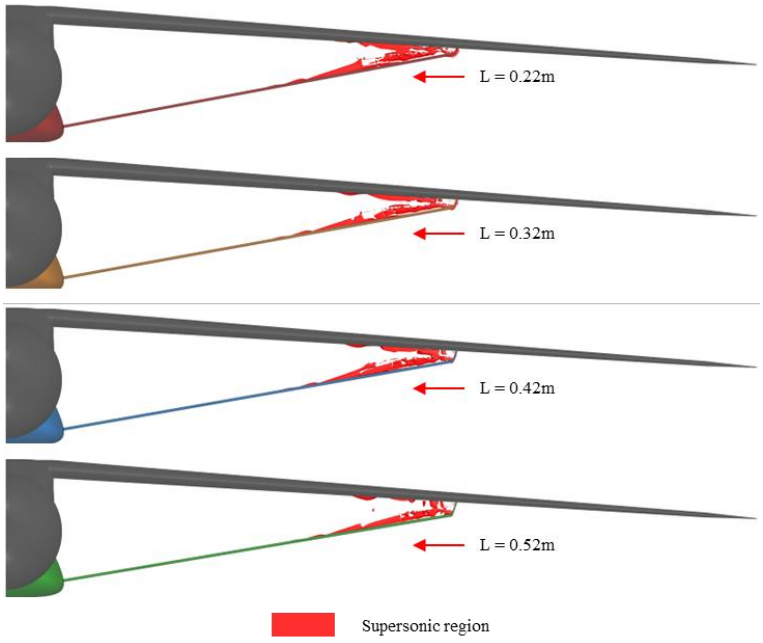

Fig. 3.21. Influence of the length parameter L on the supersonic region at α=1°

Fig. 3.22 illustrates the variation of the pressure coefficient distribution along the wing's lower surface as a function of the angle of attack α for the reference case. As α increases, both the size and intensity of the shock wave along the spanwise direction decrease. This behavior is attributed to changes in the pressure distribution induced by the altered flow conditions. At higher angles of attack, the pressure gradient along the flow direction on the wing's lower surface decreases, resulting in a reduction of the shock wave intensity. This trend reflects the overall deceleration of the flow within the channel formed between the wing and the strut.

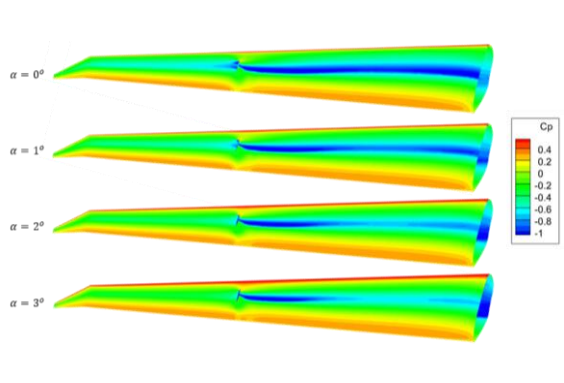

Fig. 3.22. Pressure coefficient distribution on the wing lower surface as a function of α

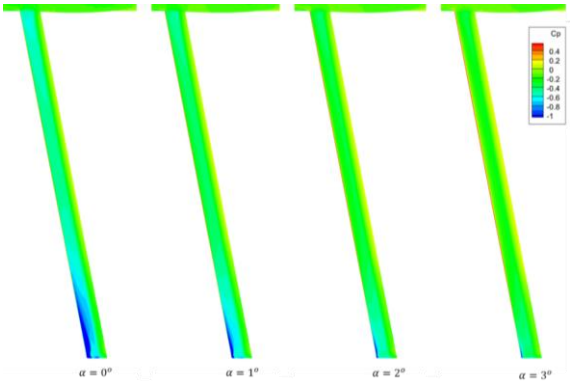

Fig. 3.23. Pressure coefficient distribution on the strut upper surface as a function of α

Similarly, analyzing the pressure coefficient distribution in Fig. 3.23 on the strut's upper surface shows a progressive reduction in shock intensity as the angle of attack increases. This attenuation can be attributed to the decreased interaction between the shocks generated on the wing's lower surface and those on the strut's upper surface. Thus, increasing the angle of attack alters the flow configuration in the wing–strut interference region, reducing both fluid acceleration and shock wave intensity.

Based on the conclusions of the previous parametric study, a two-dimensional optimization of the strut airfoil geometry was carried out, aiming to reduce fluid acceleration in the channel between the strut and the wing. For this process, the reference section was chosen at Y=15m, representing a compromise between the effects of shock interactions and the influence of spanwise flow accentuated by the wing-strut junction geometry. The selected section is illustrated in Fig. 3.24.

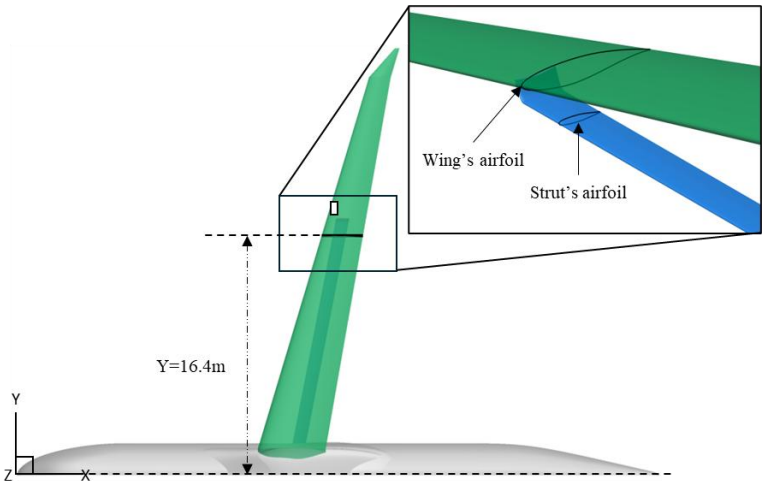

Fig. 3.24. Y=15m section

In this case, the optimization process involved seven control parameters (CST weights and the local angle of attack of the strut), so a complete gradient evaluation required eight aerodynamic analyses per iteration: one for the current objective function value and one for each parameter perturbation. Additionally, a minimum area constraint was imposed to avoid structurally unfeasible geometries. The mathematical formulation of the imposed problem is:

$$\begin{aligned} &Minimize: f(x) = C_D \\ &subjected\ to: S_{opt} \geq 0.9 \cdot S_{ref} \end{aligned} \tag{3.3}$$

The convergence history of the optimization shows a reduction in the aerodynamic drag coefficient by approximately 28%, while respecting the minimum area constraint of the strut

profile. The lift coefficient decreased by about 24%, indicating that the strut's influence on the overall configuration is minor. The performance improvement is attributed to the locally optimized strut incidence angle, which reduced fluid acceleration in the wing–strut channel. This optimization was performed without considering three-dimensional effects, such as spanwise flow or wing–strut junction geometry. Subsequently, the aircraft configuration with the optimized strut was analyzed and compared with the reference configuration, maintaining the same airfoil geometry and a constant local incidence. Fig. 3.25 presents the variation of aerodynamic characteristics vs. angle of attack for the optimized configuration in comparison with the results from the parametric study.

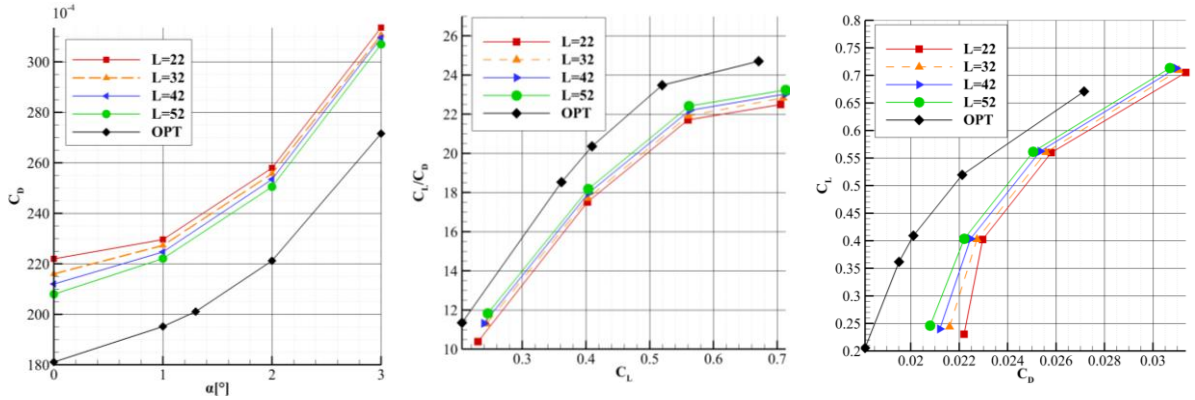

Fig. 3.25. Variation of C_D vs α (a), C_L/C_D vs C_L (b) și C_L vs C_D (c) for the two-dimensional optimized configuration compared with the results from the strut parametric study.

Fig. 3.26 illustrates the supersonic regions for both the optimized configuration and the reference configuration. A substantial reduction of the supersonic area is observed in the optimized configuration, being almost completely eliminated along the wingspan, except for the region adjacent to the wing–strut junction.

Fig. 3.26. Representation of the supersonic regions for both the initial and optimized configurations

Comparing the pressure coefficient (C_p) distribution on the wing's lower surface between the optimized configuration and the reference geometry, a significant reduction in shock intensity along the entire wing is observed, except in the region adjacent to the strut junction. The results highlight the importance of the optimized strut airfoil geometry in mitigating the effects of shock-wave interactions within the wing–strut channel, contributing to an overall reduction in aerodynamic drag. Additionally, the potential for further improvements is emphasized through local optimization of the junction region, where three-dimensional effects and the influence of transverse geometry could be incorporated into the optimization process.

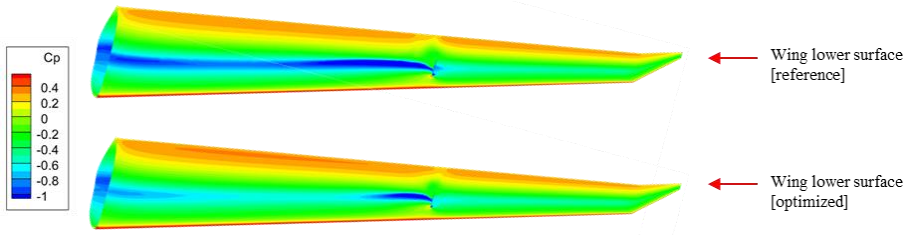

Fig. 3.27. Pressure coefficient distribution on the lower surface of the reference and optimized wings

For a better understanding of the phenomenon, three representative regions were selected, as shown in Fig. 3.28, to analyze the evolution of the pressure coefficient distribution along the spanwise position of the section. The regions correspond to a spanwise location of Y=16.4 m in the wing–strut junction area, Y=15 m in the area where the two-dimensional optimization was performed, and Y=14 m in the outer region beyond the supersonic zone in the optimized configuration.

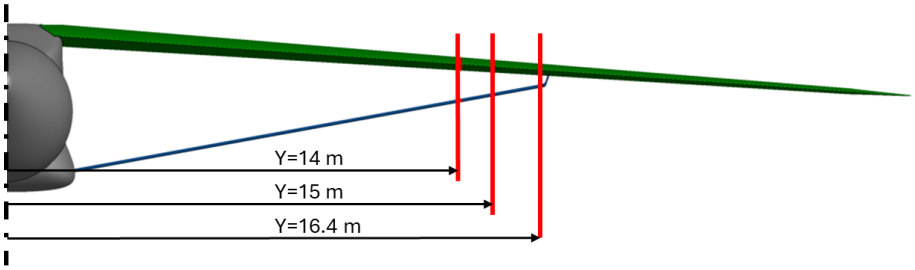

Fig. 3.28. Analyzed sections of interest

The pressure coefficient distribution on the three analyzed sections, presented in Fig. 3.29, highlights a significant reduction in the intensity of shock-wave interactions between the optimized and reference configurations. The effectiveness of the optimization becomes increasingly evident as the sections move away from the wing–strut junction region, where three-dimensional flow effects along the spanwise direction become dominant.

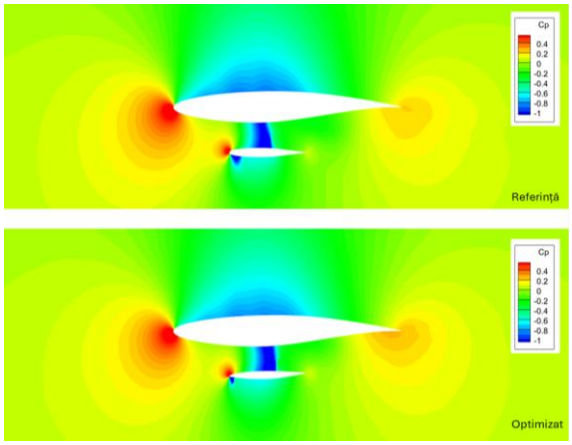

(a) Y=16.4m

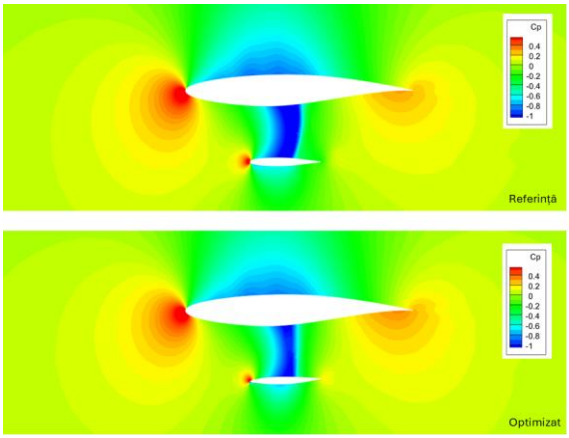

(b) Y=15m

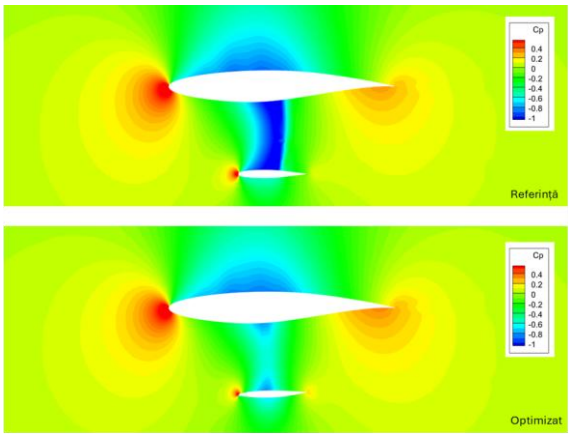

(a) Y=14m

Fig. 3.29. Pressure coefficient distribution in the selected sections: (a) Y=16.4m, (b) Y=15m, (c) Y=14m

Based on the results of the two-dimensional optimization of the strut, a procedure was developed to include the geometry of the strut junction region in the optimization. Given the high computational effort required for full-scale simulations, the methodology was designed as a compromise between fidelity and computational cost. A grid deformation method was applied, allowing local geometry modifications without the need to regenerate the entire computational mesh, thereby reducing the evaluation time of the objective function. For efficiency, the computational domain was restricted to the strut junction region, with symmetry planes placed in areas with minimal three-dimensional effects, ensuring high simulation fidelity. The analyzed section spans 5 m in width and extends along Y = 13–18 m. Although this approach does not fully reproduce the flow behavior of the entire configuration, the balance between simulation fidelity and reduced computational effort renders it feasible within the available resources.

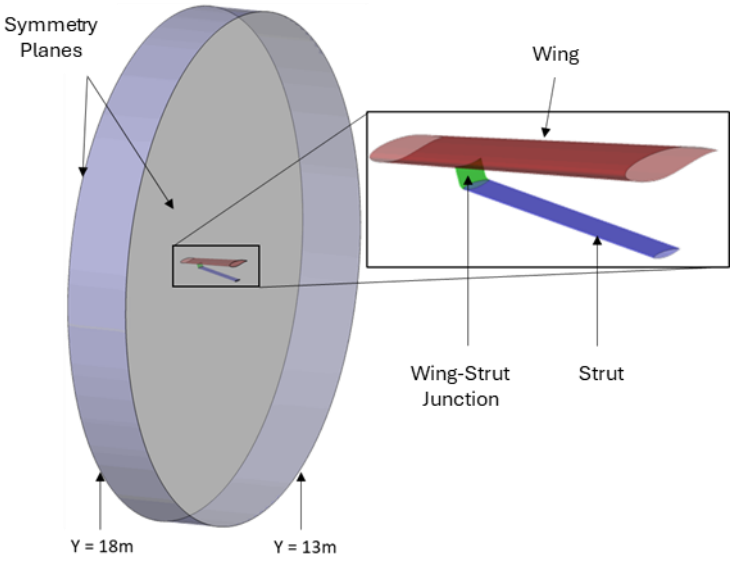

Fig. 3.30. Geometric representation of the section used in the aerodynamic optimization process

The geometry was parameterized using the volume deformation technique, treating the grid nodes as optimization parameters, which allows exploration of a restricted configuration space. Using the previous solution as a starting point significantly reduces convergence time. The main drawback is the high number of variables, managed by constraining node displacements to the vertical direction only. The control points employed in the optimization

enable local adjustments with a maximum amplitude of ±0.015 m, maintaining the consistency and stability of the computational grid.

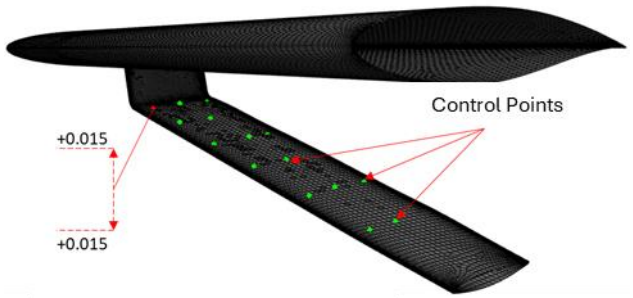

Fig. 3.31. Representation of the control points on the upper surface of the strut

In Fig. 3.32, the variations of the drag coefficient C_D and lift coefficient C_L as functions of the angle of attack α are presented. It is observed that the shock-wave interactions in the strut–wing junction region produce an almost parallel shift in the drag curve compared to both the 2D optimized configuration and the reference configuration.

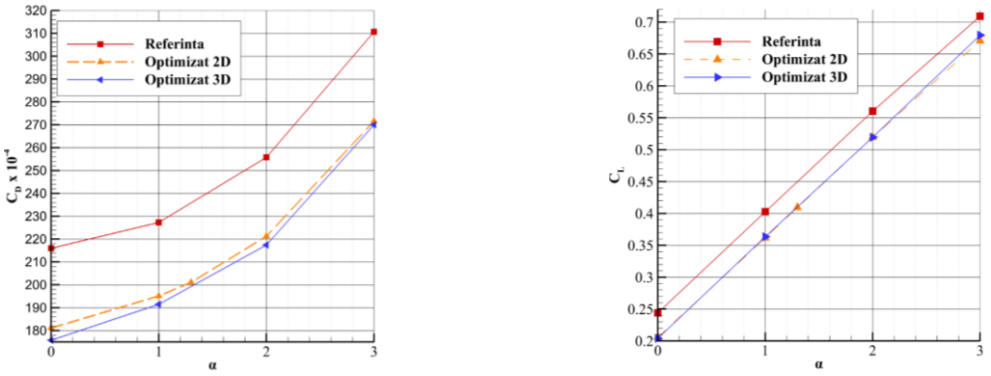

(a) (b)

Fig. 3.32. Variation of C_D vs α (a) și C_L vs α (b) for the three-dimensional optimized configuration compared with the two-dimensional optimized and reference configurations

For a deeper understanding of the optimization effects on aerodynamic characteristics, two types of flow physics representations were performed. In the first stage, the sizes of the supersonic regions were compared for the three configurations: reference, two-dimensional optimized, and three-dimensional optimized. This approach highlights the chosen methodology by progressively presenting the results, starting from the reference configuration, followed by the 2D optimized configuration, and finally the 3D optimized configuration.

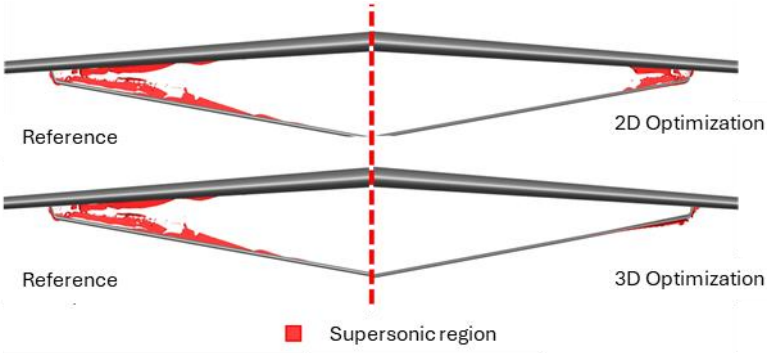

Fig. 3.33. Representation of the supersonic regions for the three-dimensional and two-dimensional optimized configurations compared to the reference configuration

The two-dimensional optimization significantly reduced the supersonic region in the mid-section of the strut; however, shock-wave interactions between the wing's lower surface

and the strut's upper surface remained partially present near the junction area. In contrast, the three-dimensional optimization completely eliminated these interactions, achieving a more uniform pressure distribution, although it induced localized accelerations on the strut's lower surface and minimal supersonic regions. Analysis of the pressure coefficient (C_p) distribution along the wing lower surface and strut upper surface shows that the three-dimensional optimization fully suppresses the shock waves, whereas the two-dimensional optimization only partially attenuates them. Near the trailing edge, a progressive flow deceleration is observed, depending on the type of optimization applied, as a result of shock-wave reduction or elimination. The C_p distribution on the strut upper surface highlights the complete removal of shock intensity in the three-dimensional optimized geometry, while in the two-dimensional case, some residual effects remain. Compared to the reference geometry, where shock locations are marked by steep pressure gradients, both optimizations significantly reduce fluid acceleration.

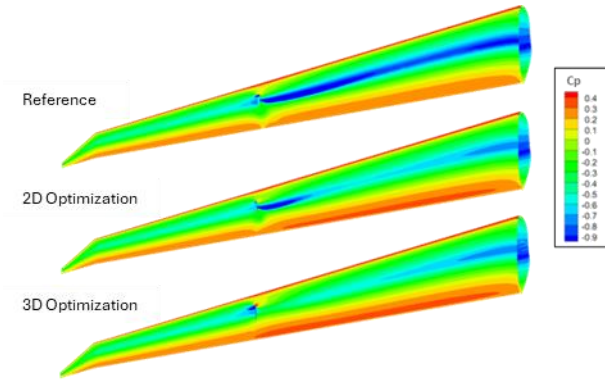

Fig. 3.34. Pressure coefficient distribution on the wing's lower surface for the three analyzed configurations

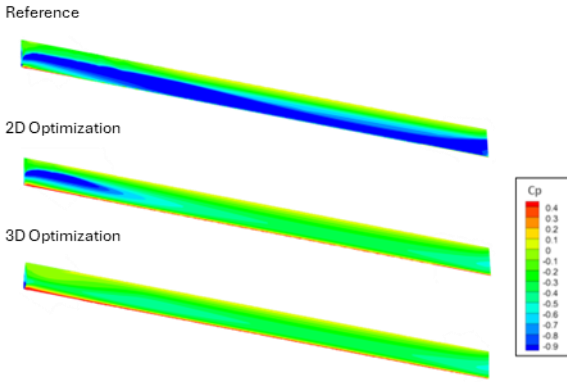

Fig. 3.35. Pressure coefficient distribution on the strut's upper surface for the three analyzed configurations

Although the three-dimensional optimization eliminated shock waves on the strut upper surface, the representations of supersonic regions show their presence on the strut lower surface. This phenomenon is attributed to the negative local incidence of the strut and the significant curvature changes in the airfoil near the strut-wing junction, which induce flow acceleration along the strut's lower surface.

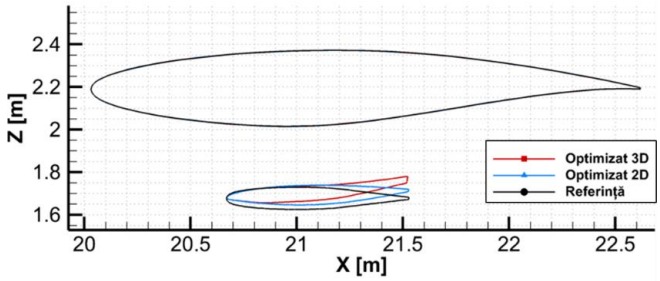

Fig. 3.36. Representation of the optimized strut profiles at the Y=16.4m section

In the case of the channel geometry, a direct relationship is observed between the optimized strut profile shapes and the channel cross-sectional area. This behavior is correlated with the area rule, expressed by the following relationship:

$$\frac{dA}{A} = (M^2 - 1) \cdot \frac{du}{u} \tag{3.4}$$

In Fig. 3.37, the variation of the cross-sectional area between the strut upper surface and the wing lower surface is illustrated. It can be observed that the reduction in drag is closely

correlated with the previously mentioned area rule. Thus, a smoother variation of the cross-sectional area along the flow path prevents local fluid acceleration, thereby contributing to the elimination of shock wave formation.

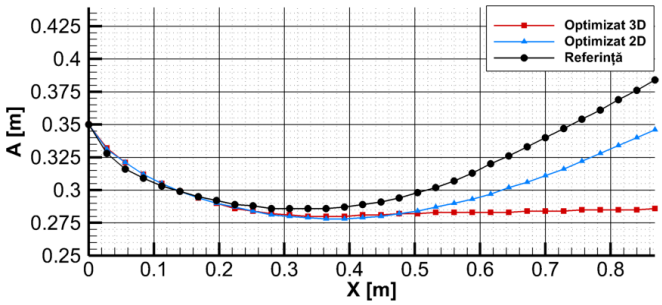

Fig. 3.37. Variation of the channel cross-sectional area along the flow direction for the reference configuration, the two-dimensional optimized configuration, and the three-dimensional optimized configuration at Y = 16.4 m.

In the case of the critical section at Y = 16.4 m, the analysis of the pressure coefficient distribution indicates a complete elimination of shock wave interactions. This is achieved by reducing the local incidence of the airfoil through curvature adjustments near the trailing edge, such that the variation of the cross-sectional area tends toward zero.

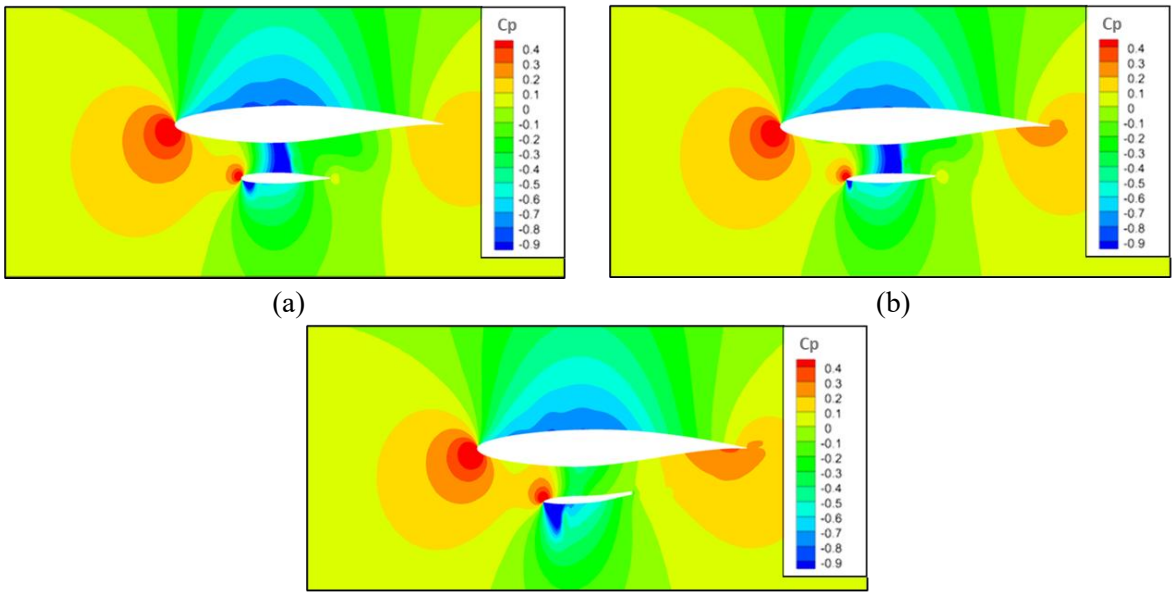

Fig. 3.38. Pressure coefficient distribution in the critical section at Y = 16.4 m for (a) the reference configuration, (b) the two-dimensional optimized configuration, and (c) the three-dimensional optimized configuration.

The continuation of the optimization study of the PADRI reference configuration focused on assessing the influence of the nacelle, positioned upstream of the wing–strut junction region, on the overall aerodynamic behavior. The nacelle geometry was integrated into both the reference and the optimized configurations, enabling a comparative evaluation of its impact on aerodynamic performance. The analysis targeted off-design flight conditions, examining the variation of aerodynamic characteristics as a function of the Mach number for the complete wing–fuselage–strut assembly.

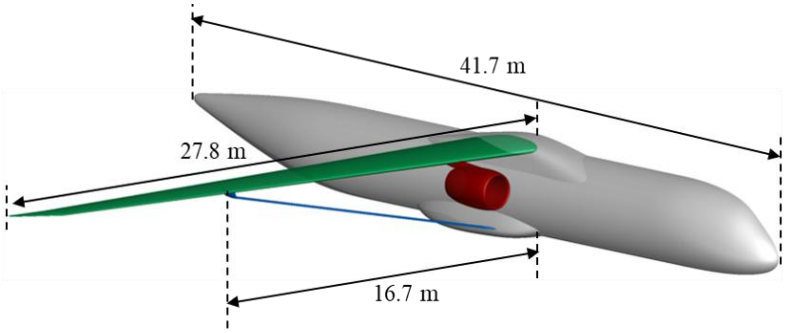

Fig. 3.39. Geometric representation of the reference configuration with the nacelle integrated

The analysis of the lift and drag coefficients as a function of the angle of attack at M=0.72 highlights the influence of the nacelle on aerodynamic performance. In the reference configuration, the presence of the nacelle reduces the lift coefficient by up to 9%, whereas in the optimized configuration, the maximum loss is reduced to 5%, with the effect progressively decreasing as the angle of attack increases.

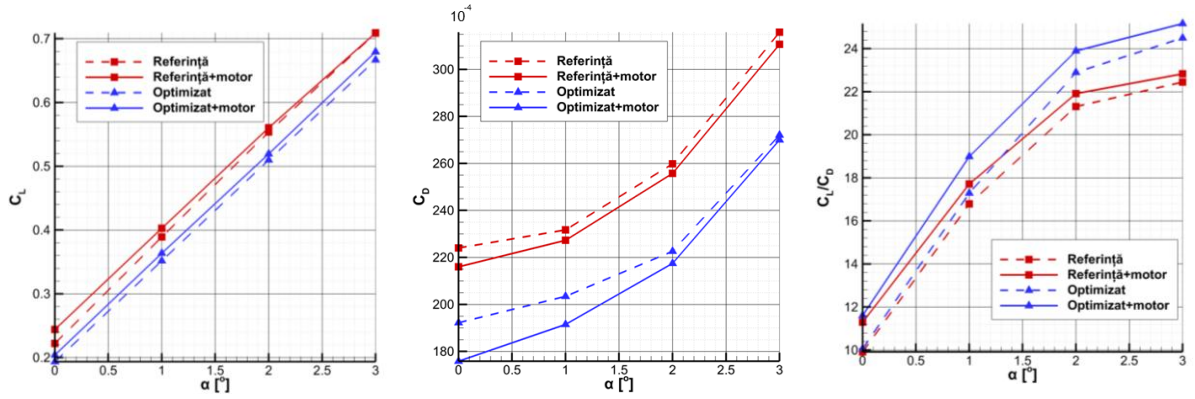

(a) (b) (c)

Fig. 3.40. Variation of C_L vs α (a), C_D vs α (b), C_L/C_D vs α (c) for both reference and optimized configuration

Regarding drag, the presence of the nacelle induces an increase of up to 3.5% for the reference configuration and up to 8.5% for the optimized configuration, with its influence diminishing as the angle of attack increases.

The analysis of aerodynamic efficiency indicates a quasi-parallel behavior between the configurations with and without the nacelle. The penalty associated with the presence of the nacelle is more pronounced for the optimized configuration, reaching up to 18 drag counts, compared to approximately 6 drag counts for the reference configuration. However, for the optimized configuration, this penalty decreases with increasing angle of attack, whereas for the reference configuration, the drag increment remains nearly constant.

The distributions of dimensionless lift forces were evaluated for the entire configuration as well as for individual components (wing, nacelle, and strut) across four angles of attack, highlighting the local impact of component interactions on aerodynamic performance.

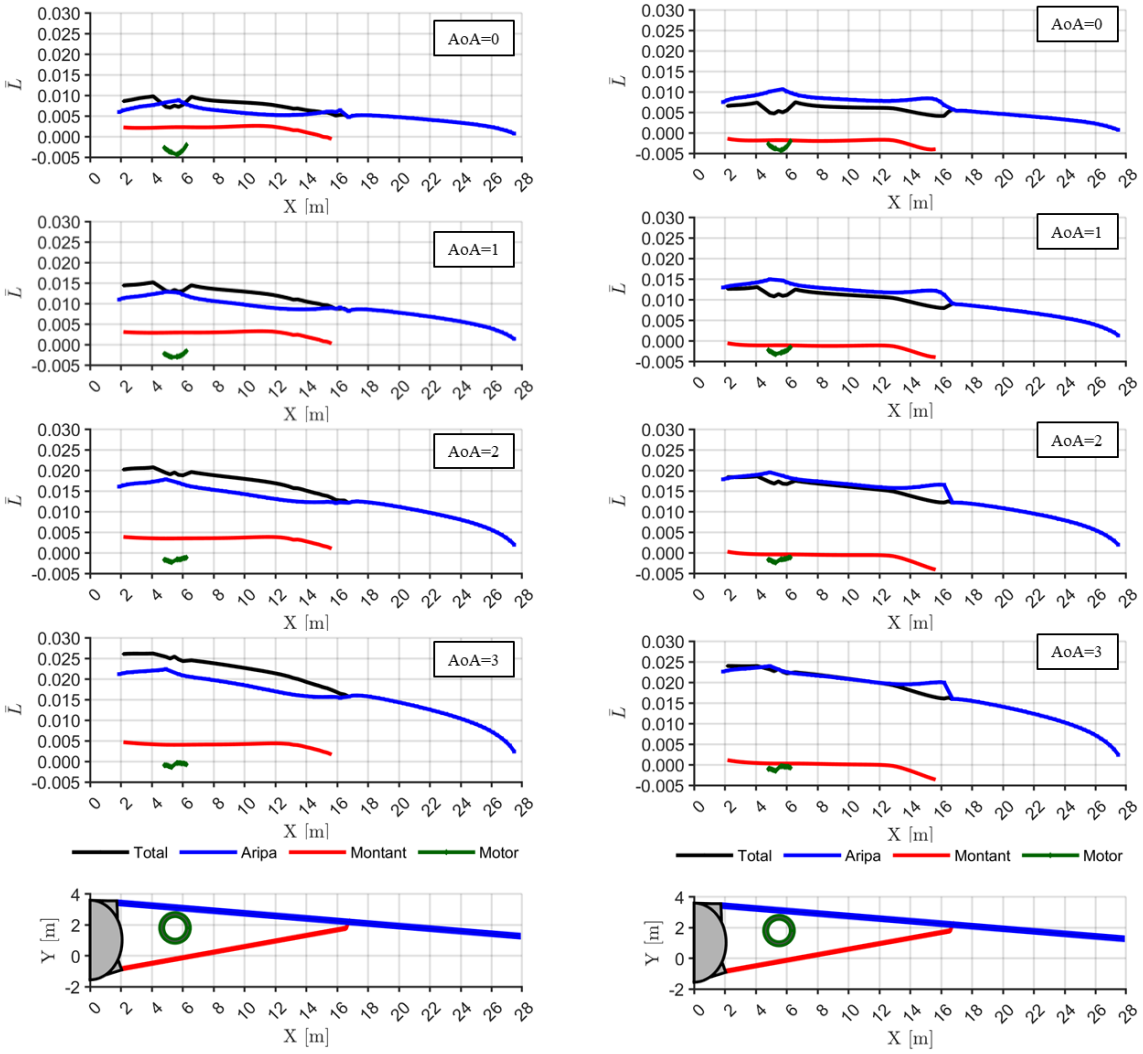

(a) Reference configuration (b) Optimized configuration

Fig. 3.41. Comparison of the non-dimensional lift force distributions for the reference and optimized configurations, highlighting the individual contributions of the main components: wing, nacelle, and strut as a function of angle of attack.

In the off-design analysis, the variation of aerodynamic coefficients with Mach number enabled identification of the critical drag-rise regime. The lift coefficient of the reference configuration increases with Mach number, while the optimized configuration exhibits a moderated increase up to M = 0.74, followed by an almost constant trend between M = 0.74–0.76 and a decrease at M = 0.78.

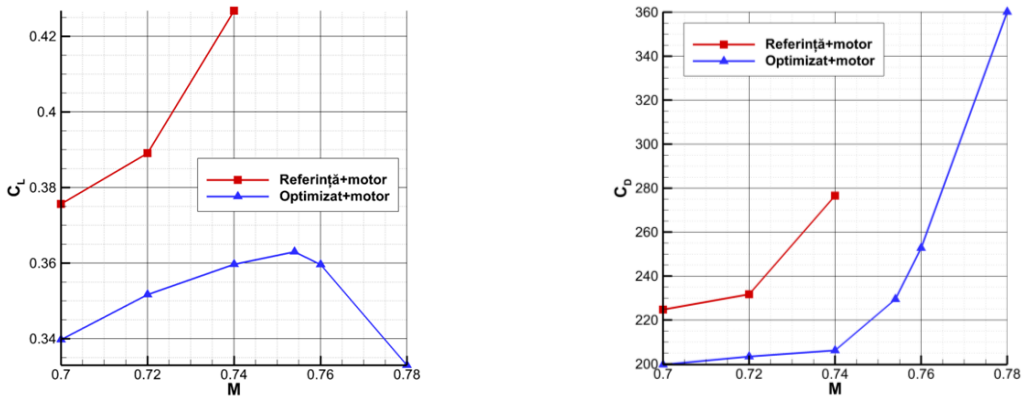

Fig. 3.42. Variation of C_L vs M (a) and C_D vs M (b) for both reference and optimized configuration

The analysis of the drag coefficient highlights significant differences between the reference and optimized configurations. For the reference configuration, the drag coefficient exhibits an exponential increase starting at M = 0.72, reflecting amplified compressibility effects and shock-wave formation associated with the drag-rise phenomenon. In contrast, the optimized configuration shows an almost constant drag up to M = 0.74, followed by a delayed increase, indicating a postponement of shock-wave interactions between the strut and the wing and maintaining a lower rate of drag growth. Analyses at M = 0.76 and M = 0.78 were conducted to identify the onset of the drag-rise phenomenon in the optimized configuration.

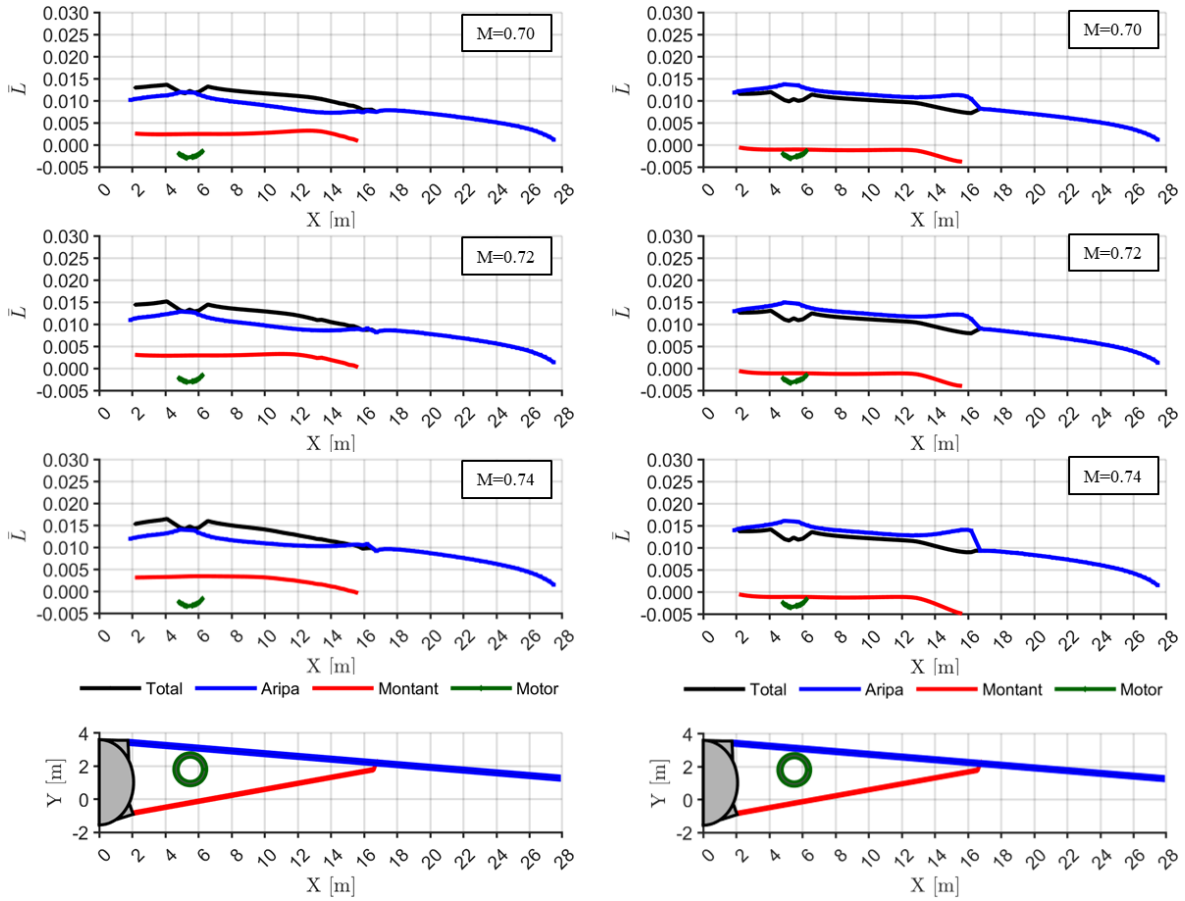

(a) Reference configuration (b) Optimized configuration

Fig. 3.43. Comparison of the non-dimensional lift force distributions for the reference and optimized configurations, highlighting the individual contributions of the main components: wing, nacelle, and strut as a function of Mach number

CONCLUSIONS

3.3 RESULTS

In conclusion, this study presents the results of developing a feasible aerodynamic and computational methodology for local transonic aerodynamic optimization of an unconventional high-aspect-ratio strut braced wing aricraft. The work highlights the importance and contribution of each stage, beginning with the development of the optimization algorithm code, followed by the analysis of the influence of the aerodynamic solver fidelity on the objective function behavior, and culminating with the application of two-dimensional and three-dimensional optimization methods in transonic flow for the strut braced wing configuration.

Chapter 1 outlines the general foundations of the work, including the motivation for the research topic and the specific objectives of the study. The chapter also details the overall structure of the thesis, highlighting the sequential steps required to approach the aerodynamic optimization process in the transonic regime for an unconventional strut braced wing aircraft.

Chapter 2 synthesizes the historical evolution, current context, and theoretical foundations relevant to the aerodynamic optimization process. Subchapter 2.1, titled *Brief Historical Overview*, analyzes the development of studies on wing–strut aircraft, presenting early examples and a chronological review of research progress. This provides the basis for understanding the current research context. Subchapter 2.2, *Current Status*, summarizes recent contributions and ongoing research directions. Subchapter 2.3, *Theoretical Foundations*, is structured into several sections. Section 2.3.1, *Parameterization Methods*, reviews the parameterization techniques for airfoils and wings, highlighting the advantages and limitations of each approach. Section 2.3.2, *Discretization Methods*, presents current mesh generation techniques used in high-fidelity aerodynamic optimization. Section 2.3.3, *Computational Models*, describes the theoretical basis of models ranging from low to high-fidelity, including assumptions and applicability. Section 2.3.4, *Optimization Algorithms*, presents deterministic and stochastic algorithms, including the theoretical framework behind the differential evolution algorithm with a parameter-free penalty scheme implemented in this study.

Chapter 3 provides a detailed analysis of the processes and results obtained in the aerodynamic optimization of the studied configuration, using both low and high-fidelity computational models. This chapter includes the development and validation of optimization methods, automation of aerodynamic evaluations, studies on the influence of solver fidelity on the objective function, and investigations into the use of neural networks in aerodynamic optimization. Results are validated through comparisons with experimental and numerical data from the literature.

Subchapter 3.1, *Comparative Study of Low and High-Fidelity Simulations*, presents an extensive investigation into the rationale for selecting the computational model for the optimization process. Section 3.1.1, *Optimization Algorithm Validation*, describes the validation of the implemented differential evolution algorithm using standard benchmark functions, with comparisons to MATLAB's genetic algorithm highlighting the advantages of the implemented solution. Section 3.1.2, *Evaluation and Automation Procedures*, details the steps for computing the objective function using XFOIL and Fluent, including geometry generation, mesh creation, and aerodynamic evaluation. Section 3.1.3, *Airfoil Optimization Results*, presents the differences between outcomes obtained using models of different fidelity

and validates the developed algorithm against MATLAB's genetic algorithm. A parametric study of the computational domain further assesses the influence of solver fidelity on objective function behavior. Section 3.1.4, *Neural Network Training Results*, reports on the feasibility of using neural networks with the generated database. Section 3.1.5, *Two-Dimensional Transonic Optimization*, validates the aerodynamic analysis against experimental and numerical reference data, followed by the results of the optimization process.

Subchapter 3.2, *PADRI Configuration Optimization*, presents the results of optimizing a reference test configuration from the literature for a wing–strut aircraft. Section 3.2.1, *PADRI Configuration Analysis*, validates numerical simulations via literature comparisons and grid convergence studies. Section 3.2.2, *Parametric Study of the Wing–Strut Junction Geometry*, presents the effects of strut length and tilt angle on aerodynamic performance, including both quantitative and qualitative assessments of supersonic inclusions and pressure distributions. Section 3.2.3, *Two-Dimensional Strut Optimization*, reports the results of optimizing the strut profile in the presence of the wing, using CST weights and local strut incidence as design variables. Section 3.2.4, *Three-Dimensional Strut Optimization*, presents the results of the full 3D aerodynamic optimization considering the junction geometry, achieving a 12.6% reduction in drag at the same lift coefficient. Qualitative results illustrate the evolution of pressure distributions and the elimination of supersonic inclusions between the wing and strut.

Subchapter 3.3, *Nacelle Influence and Off-Design Studies*, provides a detailed analysis of the aerodynamic impact of adding a nacelle upstream of the wing–strut region. Section 3.3.1, *Nacelle Influence Studies*, investigates the effects on lift distribution for several angles of attack, highlighting component-wise contributions. Section 3.3.2, *Off-Design Aerodynamic Characteristics*, compares the optimized configuration with nacelle and the reference configuration with nacelle across multiple off-design flight regimes, assessing both total and component-wise lift distributions and interactions.

This comprehensive study demonstrates the feasibility of a methodical aerodynamic optimization process for unconventional wing–strut aircraft in the transonic regime, offering both computational efficiency and high-fidelity results.

3.4 ORIGINAL CONTRIBUTIONS

The original contributions of this thesis are summarized as follows:

1. Development and implementation of a constrained differential evolution optimization algorithm applied in aerodynamic optimization processes. The validation and application of this algorithm are detailed in Sections 3.1.1 (*Validation of the optimization algorithm*), 3.1.3 (*Airfoil optimization results*), and 3.1.5 (*Two-dimensional transonic optimization*). These results have also been presented in scientific papers and conference contributions listed in Sections 4.4.1 (*List of scientific publications*) and 4.4.2 (*List of technical and scientific presentations*).
2. Development of automation codes called by the objective functions during high-fidelity optimization processes using solvers such as Fluent and ADFlow. These codes employ a multi-language coupling approach (Python, JavaScript, and MATLAB) and are described in Sections 3.1.2 (*Evaluation and aerodynamic automation procedures*) and 3.1.5 (*Two-dimensional transonic optimization*), with results also presented in the publications and conferences mentioned above.

3. Detailed comparative analysis of the influence of aerodynamic solver fidelity on objective function behavior and, consequently, on the optimization outcomes, as presented in Section 3.1.3. These findings have also been disseminated through scientific papers and conference contributions.
4. Generation of a high-fidelity aerodynamic database extensive enough to train a neural network, along with a feasibility study for its application in aerodynamic optimization, described in Section 3.1.4 (*Neural network training results*) and presented in scientific conferences and publications.
5. Parametric study of the influence of strut junction length and fillet radius on the aerodynamic characteristics of the PADRI configuration, detailed in Section 3.2.2 (*Parametric study of the wing–strut junction geometry*) and reported in scientific articles and conference presentations.
6. Determination of the effect of local strut incidence and cross-sectional area variations between the strut and wing on shock-wave interactions within the PADRI configuration, as detailed in Sections 3.2.3 (*Two-dimensional strut optimization*) and 3.2.4 (*Three-dimensional strut optimization*), with results presented at scientific conferences and in journal publications.
7. Analysis of the nacelle geometry influence and off-design behavior for both the PADRI reference configuration and the optimized configuration, as detailed in Subchapter 3.3 (*Nacelle influence and off-design studies*).
8. Publication of eight original scientific articles arising from the research conducted within this thesis.

3.5 FUTURE DEVELOPMENT PERSPECTIVES

This work proposes two major directions for future research, aimed at extending and enhancing the current aerodynamic optimization methodology and contributing to the design of next-generation aerospace configurations.

The first direction focuses on the implementation of passive or active flow control methods applied to the reference configuration. The primary objective is to eliminate or reduce flow separation zones induced by shock waves and to attenuate the interactions between shock waves generated in the wing–strut junction, which are critical regions in terms of aerodynamic efficiency. Passive control, through the introduction of devices such as micro-vortex generators, represents a technologically straightforward solution, offering the advantage of reducing separation regions. In parallel, active control methods, such as suction or fluid injection, provide a higher degree of adaptability to varying flight conditions, allowing local flow modifications. This research direction also opens the possibility of hybrid combinations of passive and active methods, with the potential to maximize flow control efficiency depending on operational conditions. Additionally, future investigations may include local modifications of the wing airfoil and simultaneous aerodynamic optimizations of both the wing and strut, aiming to identify integrated solutions that minimize adverse shock-wave effects and improve overall aerodynamic efficiency.

The second development perspective targets the integration of structural evaluation within the aerodynamic optimization process, transforming the current methodology into a multidisciplinary aero-structural approach. In this framework, optimization would not only aim

at reducing drag or maximizing lift but also ensure compliance with constraints related to weight, structural strength, and manufacturability. However, this extension significantly increases the computational cost, as structural analysis requires the generation and evaluation of a large number of configurations, each necessitating detailed aerodynamic and structural simulations. Accordingly, the development of automated processes for generating and analyzing the internal structure of the wing and strut becomes essential.

This integrated approach could lead to the design of efficient configurations that meet stringent aviation requirements, such as reduced fuel consumption, lower carbon emissions, and enhanced sustainability. Furthermore, the results obtained could be extrapolated to other unconventional configurations, including flying-wing aircraft or Prandtl-type wing designs.

3.6 LIST OF PUBLICATIONS AND PRESENTATIONS

3.6.1 List of Scientific Publications

During the PhD research, eight scientific articles relevant to the topic of this thesis were prepared and published, as follows:

1.	**Hothazie, M.-V.**, Crunțeanu, D.-E., Pricop, M.-V., & Bunescu, I. (2025), "*Exploring the Impact of Strut Geometry on Strut-Braced Wing Configurations",* MDPI Aerospace, 12(6), 473.
2.	**Hothazie, M.-V.**, Crunțeanu, D.-E., Pricop, M.-V., Bunescu, I., Negoiță M.-F., & Stoican M.-G. (2023), *"Design Exploration of the NACA Airfoil Family Using High-Fidelity CFD Analysis"*, INCAS BULLETIN, Volume 17, Issue 2/ 2025, pp. 35 – 45
3.	**Hothazie, M.-V.**, Crunțeanu, D.-E., Pricop, M.-V., Bunescu, I. & Stoican M.-G. (2024), *"CFD Numerical Simulations of the Strut Braced Wing Configuration using Overset Grid Technique",* AIP, in press.
4.	**Hothazie, M.-V.**, Crunțeanu, D.-E., Pricop, M.-V., & Bunescu, I. (2023), *"Studies Regarding Aerodynamic Optimization Processes of Supercritical Airfoils",* AIP, in press.
5.	**Hothazie, M.-V.**, Crunțeanu, D.-E., Pricop, M.-V., Bunescu, I. & Onel A.-O. (2023), *"Studies Regarding the Aerodynamic Performance of Truss-Braced Wing Configurations in Transonic Regime ",* AIP, in press.
6.	**Hothazie, M.-V.,** Bunescu, I., Stoican M.-G. & Chelemen D.-S. (2024), *"Investigating the Effectiveness of Vortex Generators in Aviation through High-Fidelity CFD Analysis*", INCAS BULLETIN, Volume 16, Issue 3/ 2024, pp. 51 – 60
7.	Negoita M.-F. & **Hothazie, M.-V.** (2024) *"A Machine Learning-Based Approach for Predicting Aerodynamic Coefficients Using Deep Neural Networks and CFD Data"*, INCAS BULLETIN, Volume 16, Issue 4/ 2024, pp. 91 – 104
8.	Negoita M.-F., Crunțeanu, D.-E., **Hothazie, M.-V.**, & Pricop, M.-V., (2023) *"Enhancing Airfoil Performance through Artificial Neural Networks and Genetic Algorithm Optimization"*, INCAS BULLETIN, Volume 15, Issue 4/ 2023, pp. 199 – 209

Among these, Article 1 has been published in a WoS-indexed journal; Articles 3, 4, and 5 are currently in publication in WoS-indexed journals; while Articles 2, 6, 7, and 8 have been published in the INCAS BULLETIN, which is indexed in BDI.

3.6.2 List of Technical and Scientific Presentations

During the doctoral studies, the author delivered 8 presentations at international scientific events, as detailed below:

1.	**Hothazie, M.-V.**, Crunțeanu, D.-E., Pricop, M.-V., & Bunescu, I. "*Exploring the Impact of Strut Geometry on Strut-Braced Wing Configurations", AIAA Sci-Tech Forum, Hyatt Regency Orlando Orlando, FL, Ianuarie 2025.*
2.	**Hothazie, M.-V.**, Crunțeanu, D.-E., Pricop, M.-V., Bunescu, I., Stoican, M.-G., & Chelemen, D.-Ș *"Strut Braced Wing Configuration Investigation Using High-Fidelity CFD Analysis"*, *International Conference of Aerospace Sciences, Bucharest, Romania, 17-18 October 2024.*
3.	**Hothazie, M.-V.**, Crunțeanu, D.-E., Pricop, M.-V., Bunescu, I. & Stoican M.-G., *"CFD Numerical Simulations of the Strut Braced Wing Configuration using Overset Grid Technique", The 22nd International Conference of Numerical Analysis and Applied Mathematics, Crete, Greece, 16 – 22 September 2024.*
4.	**Hothazie, M.-V.**, Crunțeanu, D.-E., Pricop, M.-V., Bunescu, I. & Stoican, M.-G., "*Investigating Truss-Braced Wing Configuration through CFD Based Analysis*", *The 9th European Congress on Computational Methods in Applied Sciences and Engineering, ECCOMAS Congress 2024*, *Lisbon, Portugal, 3 – 7 June 2024.*
5.	**Hothazie, M.-V.**, Crunțeanu, D.-E., Pricop, M.-V., Bunescu, I. & Stoican M.-G., *"Studies Regarding the Aerodynamic Performance of Truss-Braced Wing Configurations in Transonic Regime ", The 21st International Conference of Numerical Analysis and Applied Mathematics, Crete, Greece, 16 – 22 September 2023.*
6.	**Hothazie, M.-V.**, Crunțeanu, D.-E., Pricop, M.-V., & Bunescu, I. (2023), *"Studies Regarding Aerodynamic Optimization Processes of Supercritical Airfoils", ICNPAA*, Prague, Czech Republic, 27 – 30 June 2023.
7.	**Hothazie, M.-V.**, Pricop, M.-V. & Bunescu, I., "Investigating the Effectiveness of Vortex Generators in Aviation through High-Fidelity CFD Analysis", Aerospace Europe Conference 2023, Joint 10th EUCASS – 9th CEAS Conference, Switzerland, 9-13 July, 2023.
8.	**Hothazie, M.-V.**, Crunțeanu, D.-E., Pricop, M.-V., Bunescu, I. & Stoican M.-G., "Low-speed airfoil shape optimization using high-fidelity CFD analysis", *AIAA Sci-Tech Forum*, National Harbor, MD & ONLINE, 23–27 January 2023.

BIBLIOGRAPHY

[1] B. Dy, A. Meeran, S. C. Joyce, A. Agarwal, and S. Joyce, "A new world of airports: forecasting 2050 aviation networks towards sustainable adaptation," 2023. [Online]. Available: https://www.researchgate.net/publication/375912568

[2] "N+3 Aircraft Concept Designs and Trade Studies, Final Report," 2010.

[3] "Flightpath 2050 Europe's Vision for Aviation." doi: 10.2777/50266.

[4] J. E. Green, "Laminar Flow Control-Back to the Future?", [Online]. Available: http://cdiac.ornl.gov/pns/current_ghg.html,

[5] A. Kretov and D. Tiniakov, "Evaluation of the Mass and Aerodynamic Efficiency of a High Aspect Ratio Wing for Prospective Passenger Aircraft," *Aerospace*, vol. 9, no. 9, Sep. 2022, doi: 10.3390/aerospace9090497.

[6] S. Kilimtzidis and V. Kostopoulos, "Multidisciplinary structural optimization of novel high-aspect ratio composite aircraft wings," *Structural and Multidisciplinary Optimization*, vol. 66, no. 7, Jul. 2023, doi: 10.1007/s00158-023-03600-1.

[7] G. K. W. Kenway and J. R. R. A. Martins, "Multipoint high-fidelity aerostructural optimization of a transport aircraft configuration," *J Aircr*, vol. 51, no. 1, pp. 144–160, 2014, doi: 10.2514/1.C032150.

[8] G. J. Kennedy, G. W. Kenway, and J. R. R. A. Martins, "High aspect ratiowing design: Optimal aerostructural tradeoffs for the next generation of materials," in *52nd Aerospace Sciences Meeting*, American Institute of Aeronautics and Astronautics Inc., 2014. doi: 10.2514/6.2014-0596.

[9] O. Gur, M. Bhatia, J. A. Schetz, W. H. Mason, R. K. Kapania, and D. N. Mavris, "Design optimization of a truss-braced-wing transonic transport aircraft," *J Aircr*, vol. 47, no. 6, pp. 1907–1917, 2010, doi: 10.2514/1.47546.

[10] F. Gern, A. Ko, B. Grossman, R. Haftka, R. K. Kapania, and W. H. Mason, "Transport Weight Reduction through MDO: The Strut-Braced Wing Transonic Transport".

[11] D. P. Wells, "Wing Configuration Impact on Design Optimums for a Subsonic Passenger Transport."

[12] J. M. Coggin, R. K. Kapania, W. Zhao, J. A. Schetz, and V. Hodigere-Siddaramaiah, "Nonlinear aeroelastic analysis of a truss based wing wind tunnel model," in *55th AIAA/ASMe/ASCE/AHS/SC Structures, Structural Dynamics, and Materials Conference*, 2014. doi: 10.2514/6.2014-0335.

[13] M. K. Bradley and C. K. Droney, "Subsonic Ultra Green Aircraft Research Phase II: N+4 Advanced Concept Development," *NASA technical report*, no. April 2011, 2011.

[14] M. K. Bradley and C. K. Droney, "Subsonic Ultra Green Aircraft Research: Phase I Final Report," 2011. [Online]. Available: http://www.sti.nasa.gov

[15] D. P. Wells, G. M. Gatlin, J. C. June, and T. V Marien, "NASA TRANSONIC TRUSS-BRACED WING STUDIES."

[16] J. M. Grasmeyer *et al.*, "Multidisciplinary Design Optimization of a Strut-Braced Wing Aircraft with Tip-Mounted Engines," 1998.

[17] J. Xiong, N. Nguyen, and J. Fugate, "Jig twist optimization of mach 0.745 transonic truss-braced wing aircraft and high-fidelity cfd validation," in *AIAA Scitech 2020 Forum*, 2020. doi: 10.2514/6.2020-0451.

[18] J. Xiong and N. Nguyen, "Steady and Unsteady Simulations of Transonic Truss-Braced Wing Aircraft for Flight Dynamic Stability Analysis," in *AIAA AVIATION 2022 Forum*, 2022. doi: 10.2514/6.2022-4151.

[19] J. Xiong, N. T. Nguyen, and J. Fugate, "Study of Mach 0.8 Transonic Truss-Braced Wing Aircraft Wing-Strut Interference Effects," in *AIAA Scitech 2021 Forum*, Reston, Virginia: American Institute of Aeronautics and Astronautics, Jan. 2021. doi: 10.2514/6.2021-0336.

[20] G. Kenway, J. Housman, and C. Kiris, "NASA Ames Research Center Contributions to the PADRI workshop," 2017.

[21] "PADRI Workshop." Accessed: Nov. 27, 2024. [Online]. Available: https://congress.cimne.com/padri-2017/frontal/default.asp

[22] JEAN-CHRISTOPHE CARBONEL, "Hurel-Dubois aircraft and their pioneering long wings," Key.Aero.

[23] "Hurel Dubois HD34," *Oldprops.ukhome*, Jan. 12, 2014.

[24] W. Mallik, "Multidisciplinary Design Optimization and Cruise Mach Number Study of Truss-Braced Wing Aircraft," 2018, doi: 10.13140/RG.2.2.33858.02241.

[25] Graham Warwick, "Gallery: A Timeline Of The Truss-Braced Wing," *Aviation Week Network*, Feb. 07, 2020.

[26] M. K. Bradley and C. K. Droney, "Subsonic Ultra Green Aircraft Research: Phase I Final Report," 2011. [Online]. Available: http://www.sti.nasa.gov

[27] Sandie Gibbs, "In Future Aircraft Designs We 'Truss,'" *nasa.gov*, Jan. 24, 2014.

[28] Richard Schuurman, "NASA paves the way for a 737 successor," *AirInsight Group*, May 30, 2021.

[29] Graham Warwick, "Gallery: A Timeline Of The Truss-Braced Wing," *Aviation Week Network* , Feb. 07, 2020.

[30] S. Kilimtzidis and V. Kostopoulos, "Multidisciplinary structural optimization of novel high-aspect ratio composite aircraft wings," *Structural and Multidisciplinary Optimization*, vol. 66, no. 7, p. 150, Jul. 2023, doi: 10.1007/s00158-023-03600-1.

[31] R. L. Campbell, S. A. Viken, and M. N. Lynde, "Application of Passive Drag Reduction Methods to a Generic Strut-Braced Wing."

[32] N. R. Secco and J. R. R. A. Martins, "RANS-Based Aerodynamic Shape Optimization of a Strut-Braced Wing with Overset Meshes," *J Aircr*, vol. 56, no. 1, pp. 217–227, Jan. 2019, doi: 10.2514/1.C034934.

[33] E. Ting, K. W. Reynolds, N. T. Nguyen, and J. Totah, "Aerodynamic Analysis of the Truss-Braced Wing Aircraft Using Vortex-Lattice Superposition Approach," in *32nd AIAA Applied Aerodynamics Conference*, Reston, Virginia: American Institute of Aeronautics and Astronautics, Jun. 2014. doi: 10.2514/6.2014-2597.

[34] Sarah Mann, "NASA's X-66 Sustainable Aircraft Model Sails Through First Wind Tests," *nasa.gov*, Nov. 21, 2024.

[35] DLR Digital Hangar, "DLR ZEexplore Truss-Braced-Wing Turbofan," DLR.

[36] Ladson Charles L and Brooks Cuyler W, "Development of a computer program to obtain ordinates for NACA 4-digit, 4-digit modified, 5-digit, and 16 series airfoils," Nov. 1975.

[37] Snorri. Gudmundsson, *General aviation aircraft design : applied methods and procedures*. Butterworth-Heinemann, 2014.

[38] M. Belda and T. Hyhlík, "Interactive Airfoil Optimization Using Parsec Parametrization and Adjoint Method," *Applied Sciences*, vol. 14, no. 8, p. 3495, Apr. 2024, doi: 10.3390/app14083495.

[39] G. Tortora, A. Concilio, and R. Pecora, "Airfoil Shape Morphing through a Novel Parameterization and Fitting Optimization Method Based on Uniform Non-Rational B-Spline Functions," *Designs (Basel)*, vol. 7, no. 1, p. 28, Feb. 2023, doi: 10.3390/designs7010028.

[40] K. Lane and D. Marshall, "Inverse Airfoil Design Utilizing CST Parameterization," in *48th AIAA Aerospace Sciences Meeting Including the New Horizons Forum and Aerospace Exposition*,

Reston, Virigina: American Institute of Aeronautics and Astronautics, Jan. 2010. doi: 10.2514/6.2010-1228.

[41] T. Chau and D. W. Zingg, "Aerodynamic Optimization and Fuel Burn Evaluation of a Transonic Strut-Braced-Wing Single-Aisle Aircraft," *J Aircr*, vol. 60, no. 5, pp. 1638–1658, Sep. 2023, doi: 10.2514/1.C037158.

[42] B. Zhu, W. Zhang, and Y. Huang, "Energy extraction properties of a flapping wing with a deformable airfoil," *IET Renewable Power Generation*, vol. 13, no. 11, pp. 1823–1832, Aug. 2019, doi: 10.1049/iet-rpg.2018.6193.

[43] Anderegg David and Yildirim Anil, "Overset Theory: Tips and Troubleshooting ," MDO Lab.

[44] D. Li and R. Hartmann, "Adjoint-Based Error Estimation and Mesh Refinement in an Adjoint-Based Airfoil Shape Optimization of a Transonic Benchmark Problem," 2016, pp. 537–546. doi: 10.1007/978-3-319-27279-5_47.

[45] A. M. Morris, C. B. Allen, and T. C. S. Rendall, "CFD-based optimization of aerofoils using radial basis functions for domain element parameterization and mesh deformation," *Int J Numer Methods Fluids*, vol. 58, no. 8, pp. 827–860, Nov. 2008, doi: 10.1002/fld.1769.

[46] Z. Lyu, G. K. W. Kenway, and J. R. R. A. Martins, "Aerodynamic Shape Optimization Investigations of the Common Research Model Wing Benchmark," *AIAA Journal*, vol. 53, no. 4, pp. 968–985, Apr. 2015, doi: 10.2514/1.J053318.

[47] A. Jameson, L. Martinelli, and J. Vassberg, "Using Computational Fluid Dynamics For Aerodynamics- A Critical Assessment," in *23rd International Congress of Aeronautical Sciences*, Toronto Canada, Sep. 2002.

[48] J. Guerrero, "Roadmap to Lecture 5: RANS Equations, Reynolds Averaging," Mar. 2021.

[49] G. Dhiman and V. Kumar, "Spotted hyena optimizer: A novel bio-inspired based metaheuristic technique for engineering applications," *Advances in Engineering Software*, vol. 114, pp. 48–70, Dec. 2017, doi: 10.1016/j.advengsoft.2017.05.014.

[50] Thomas. Bäck, *Evolutionary algorithms in theory and practice : evolution strategies, evolutionary programming, genetic algorithms*. Oxford University Press, 2020.

[51] B. Alatas and U. Can, "Physics based Metaheuristic Optimization Algorithms for Global Optimization Physics Based Metaheuristic Algorithms for Global Optimization," 2015. [Online]. Available: http://www.aiscience.org/journal/ajischttp://creativecommons.org/licenses/by-nc/4.0/

[52] A. Darwish, "Bio-inspired computing: Algorithms review, deep analysis, and the scope of applications," *Future Computing and Informatics Journal*, vol. 3, no. 2, pp. 231–246, Dec. 2018, doi: 10.1016/j.fcij.2018.06.001.

[53] X.-S. Yang and M. Karamanoglu, "Swarm Intelligence and Bio-Inspired Computation," in *Swarm Intelligence and Bio-Inspired Computation*, Elsevier, 2013, pp. 3–23. doi: 10.1016/B978-0-12-405163-8.00001-6.

[54] Yongsheng. Ding, Lei. Chen, and Kuangrong. Hao, *Bio-inspired collaborative intelligent control and optimization*. Springer Singapore, 2018.

[55] E.-S. M. El-Alfy and A. A. Al-Hasan, "A novel bio-inspired predictive model for spam filtering based on dendritic cell algorithm," in *2014 IEEE Symposium on Computational Intelligence in Cyber Security (CICS)*, IEEE, Dec. 2014, pp. 1–7. doi: 10.1109/CICYBS.2014.7013372.

[56] S. N. Skinner and H. Zare-Behtash, "State-of-the-art in aerodynamic shape optimisation methods," *Appl Soft Comput*, vol. 62, pp. 933–962, Jan. 2018, doi: 10.1016/j.asoc.2017.09.030.

[57] Rogalsky Tim, Derksen R., and Kocabiyik S., "Differential Evolution in Aerodynamic Optimization," 1999.

[58] M.-V. HOTHAZIE, G. ICHIM, and M.-V. PRICOP, "Development and validation of constraints handling in a Differential Evolution optimizer," *INCAS BULLETIN*, vol. 12, no. 1, pp. 59–66, Mar. 2020, doi: 10.13111/2066-8201.2020.12.1.6.

[59] M. V. Hothazie, G. Ichim, and M. V. Pricop, "Development and validation of constraints handling in a differential evolution optimizer," *INCAS Bulletin*, vol. 12, no. 1, pp. 59–66, 2020, doi: 10.13111/2066-8201.2020.12.1.6.

[60] *Experimental data base for computer program assessment : report of the Fluid Dynamics Panel, Working Group 04*. North Atlantic Treaty Organization, Advisory Group for Aerospace Research and Development, 1979.

[61] C. A. Mader, G. K. W. Kenway, A. Yildirim, and J. R. R. A. Martins, "ADflow: An Open-Source Computational Fluid Dynamics Solver for Aerodynamic and Multidisciplinary Optimization," *Journal of Aerospace Information Systems*, vol. 17, no. 9, pp. 508–527, Sep. 2020, doi: 10.2514/1.I010796.